The geometry of the North Anatolian transform fault in the Sea of Marmara and its temporal evolution: implications for the development of intracontinental transform faults

A. M. Celâl Şengör, Céline Grall, Caner Imren, Xavier Le Pichon, Naci Görür, Pierre Henry, Hayrullah Karabulut, Muzaffer Siyako

THE GEOMETRY OF THE NORTH ANATOLIAN TRANSFORM FAULT IN THE SEA OF MARMARA AND ITS TEMPORAL EVOLUTION: IMPLICATIONS FOR THE DEVELOPMENT OF INTRACONTINENTAL TRANSFORM FAULTS

A. M. Celâl Şengör[1,2], Céline Grall[3], Caner İmren[4], Xavier Le Pichon[5], Naci Görür[1] Pierre Henry[3], Hayrullah Karabulut[6] , Muzaffer Siyako[7]

[1] İstanbul Teknik Üniversitesi, Maden Fakültesi, Jeoloji Bölümü, Ayazağa 34469 İstanbul TURKEY

[2] İstanbul Teknik Üniversitesi, Avrasya Yerbilimleri Enstitüsü, Ayazağa 34469 İstanbul, TURKEY

[3] CEREGE, CNRS-Aix Marseille Université, Marseille, FRANCE

[4] İstanbul Teknik Üniversitesi, Maden Fakültesi, Jeofizik Bölümü, Ayazağa 34469 İstanbul, TURKEY

[5] Professeur Honoraire au Collège de France, Europôle de l'Arbois, Bât. Trocadéro, BP 80 13 545 Aix-en-Provence cedex 04 FRANCE

[6] Kandilli Rasathanesi, Boğaziçi Üniversitesi, Kandilli, İstanbul, TURKEY

[7] Türkiye Petrolleri Anonim Ortaklığı, Arama Grubu, Ankara, TURKEY

In pietate memoriam J. Tuzo Wilson

ABSTRACT

The North Anatolian Fault is an 1200-km long strike-slip fault system connecting the East Anatolian convergent area with the Hellenic subduction zone and as such represents an intracontinental transform fault. It began forming some 13 to 11 Ma ago within a keirogen, called the North Anatolian Shear Zone, that becomes wider from east to west. Its width is maximum at the latitude of the Sea of Marmara, where it is 100 km. The Marmara Basin is unique in containing part of an active strike slip fault system in a submarine environment in which there has been active sedimentation in a Paratethyan context where stratigraphic resolution is higher than elsewhere in the Mediterranean. It is also surrounded by a long-civilised rim where historical records reach well into the second half of the first millenium BCE. In this study we have used 210 multichannel seismic reflexion profiles adding up to 6210 km profile length and high resolution bathymetry and chirp profiles reported in the literature to map all the faults that are younger than the Oligocene. Within these faults we have distinguished those that cut the surface and those which do not. Among the ones that do not cut the surface, we have further created a time-table of fault generation based on seismic sequence recognition. The results are surprising in that faults of all orientations contain subsets that are active and others that are inactive. This suggests that as the shear zone evolves, faults of all orientations become activated and deactivated in a manner that

now seems almost haphazard, but a tendency is noticed to confine the overall movement to a zone that becomes narrower with time since the inception of the shear zone, i.e. the whole keirogen, at its full width. In basins, basin margins move outward with time, whereas highs maintain their faults free of sediment cover making their dating difficult, but small perched basins on top of them in places make relative dating possible. These basins in addition permit comparison of geological history of the highs with those of the neighboring basins. The two westerly deeps within the Sea of Marmara seem inherited structures from the earlier Rhodope-Pontide fragment/Sakarya continent collision, but were much accentuated by the rise of the intervening highs during the shear evolution. When it is assumed that below 10 km depth the faults that now constitute the Marmara fault family might have widths approaching 4 km, the resulting picture resembles a large version of an amphibolite-grade shear zone fabric, an inference in agreement with the scale-independent structure of shear zones. We think that the North Anatolian Fault at depth has such a fabric not only on a meso, but also on a macro scale. Detection of such broad, vertical shear zones in Precambrian terrains may be one way to get a handle on relative plate motion directions during those remote times.

INTRODUCTION

In 1965, J. Tuzo Wilson defined a new kind of fault that could not be accounted for by Anderson's theory of faulting in a continuous medium (Anderson, 1951; Wilson's 1965

paper was also the founding paper of plate tectonics). Wilson pointed out that the new class of faults served to connect two plate boundaries (the word 'plate' is Wilson's) with one another by transforming the motion along them into another kind of motion (Fig. 1). He therefore called them 'transform faults' (Wilson, 1965). Because plate boundaries are so cleanly delineated in the oceans, there is seldom any doubt as to the nature of faulting in them, but the scattering of deformation in the continents into areas of complex strain, in places as wide as 3000 km (as in Asia now), makes it difficult to decide to what kind of fault class some of the large strike-slip faults moving in such regions should be assigned.

In the case of the North Anatolian Fault (Ketin, 1948, 1969, 1976; Pavoni, 1962; McKenzie, 1972; Şengör, 1979; Barka, 1992, 1996; Şengör et al., 2005), it is clear that it connects the East Anatolian zone of convergence (Şengör and Kidd, 1979; Dewey et al., 1986; Şengör et al., 2003; 2008) with the Hellenic Trench (Dewey & Şengör 1979, McKenzie and Jackson 1983, Le Pichon et al. 1993; Şengör 2011) and as such qualifies as a transform fault (Şengör, 1979; Le Pichon and Kreemer, 2010). It consists of a numerous family of faults going from the well-defined Karlıova Basin in the East (Şengör, 1979; Şaroğlu, 1985; Şengör et al., 1985) to the more diffuse transtensional region in the Northern Aegean (Fig. 2). Throughout its length, its various branches have been mapped in the field (see especially Herece and Akay, 2003), and it is generally agreed

77 that the broad region of deformation, a veritable keirogen[1], called the North Anatolian
78 Shear Zone (Fig. 3; Şengör et al., 2005; Le Pichon et al., in press), in which the fault now
79 moves, came into existence sometime during the later medial Miocene between the
80 Serravallian and the Tortonian (see especially Şengör et al., 2005; Görür and Elbek,
81 submitted; between the Sarmatian and the early Pannonian in the Paratethyan scale and
82 between MN7/8 and MN10 in the European mammal stages; much of the deposits
83 along the North Anatolian Shear Zone have been dated using these two latter
84 standards). What so far has been unclear is how the broad keirogen became localised
85 into the narrow, single-strand (double strand west of Yeniçağa near Bolu: Fig. 2) main
86 displacement zone(s), constituting the North Anatolian Fault. To study the manner of
87 that localisation, the Sea of Marmara appears to be an ideal location, because a large
88 number of both multi-channel seismic and chirp profiles, shallow gravity cores (down
89 to 30 m from the sea floor, some of which are now dated and enabled assessments to be
90 made of the sedimentological events recognized in them: Beck et al., 2007; Eriş et al.,
91 2012 , Çağatay et al., in press), a number of deeper hydrocarbon exploration wells,
92 recent seismic studies including the water column itself, plus a complete, detailed
93 bathymetric coverage are available (for references prior to 2005, see Şengör et al., 2005;

---

[1] A *keirogen* (from ancient Greek κειρω = shear) is abroad strike-slip shear zone in which more than one major strike-slip fault and associated structures take up the shear and it is the strike-slip counterpart of the shortening *orogens* and extending *taphrogens*. It was first defined in Şengör and Natal'in, 1996, p. 639, endnote 8)

Armijo et al., 2005; Carton, 2005; Gazioğlu et al., 2005; Cormier et al., 2006; Seeber et al., 2006; Carton et al., 2007; Dolu et al., 2007; Géli et al., 2008; Laigle et al., 2008; Bécel, 2009; Kuşçu, 2009; Bécel et al., 2010; Özeren et al., 2010; Şengör et al., 2011; Gasperini et al., 2012; Shillington et al., 2012; Sorlien et al., 2012; Zitter et al., 2012; Le Pichon et al., in press).

Moreover, the Marmara Sea and its surroundings are frequently visited by earthquakes of devastating size with tragic consequences and the long historical records kept since at least the second half of the first millennium BCE (Fig. 4) give us an unparalleled knowledge of their repeat times and natures. That yet another imminent large earthquake is now threatening İstanbul, one of the megalopolises of the world and a cultural treasure house of mankind (it is the oldest continuously inhabited human dwelling in the world, since ~250,000 BCE, when the cave dwellers discovered its advantages as a location: see Howell et al., 2010) has focused the attention of geologists, geographers and geophysicists on this Sea after the disastrous 1999 earthquakes in İzmit and Düzce in northwestern Turkey (see Şengör et al., 2005). The fact that the Marmara area has been a part alternately of the Tethyan and Paratethyan realms since the beginning of the Miocene has given it a stratigraphy of a resolution higher than the normal Tethyan regions, because of the complete and abrupt change of biotas during every transition (so far used only for the youngest sequences and for the frame of the Sea, except where well information has been released by the petroleum industry). All of

114 these factors make the Marmara region an ideal site to study the evolution of a strike-
115 slip system below it.

116 We have critically reviewed the maps of the Marmara fault segments (e.g. Parke et al.,
117 1999, 2002; Le Pichon et al., 2003; Rangin et al., 2004, Grall et al., 2012, Sorlien et al.,
118 2012) by using that database (Fig. 5A) consisting of 210 multichannel seismic reflexion
119 profiles adding up to 6210 km profile length, so far unpublished except some segments
120 of a number of the profiles that had been published by Ateş et al. (2003) and high
121 resolution bathymetry and chirp profiles reported in the literature to map all the faults
122 that appear to cut the Miocene to Recent sedimentary rocks in the Sea of Marmara. We
123 then distinguished those that cut only a portion of the sedimentary sequence and
124 tentatively established a crude sequence of faulting events, according to the state of
125 knowledge about the seismic stratigraphy of the Sea of Marmara (the crudeness being a
126 function of the local paucity of direct litho- and biostratigraphic control). Finally, we
127 have correlated the faults that cut the present-day sea-floor with the microearthquake
128 epicentres between the years 2005 and 2011 plus the fault-plane solutions of all the
129 earthquakes with magnitudes greater than 4 with a view to seeing which faults may
130 have localised motion, and, where information is available, what kind, since 1960. In the
131 sections that follow, we describe the faults illustrated in Fig. 5B and give examples of
132 various faulting events established using seismic sequence stratigraphy.

133 Stratigraphic sequences that are related to 100 ka glacial/interglacial cyclicity over the

last 450-540 ka are here depicted following the recent publications by Grall et al. (2012 and in press b) and Sorlien et al., (2012). These authors show repetitions of onlap geometries (laterally correlated with condensed sections, Grall et al., in press b), and forset/toplap geometries (Sorlien et al., 2012) and related them to variations of sedimentation rates during low-stand/high-stand transitions and low-stand deltas respectively. These authors use the following colour code associated to Marine Isotopic Stage (MIS) transitions: the Red MIS-5 (140 ka), the Blue MIS-7 (240 ka), the Yellow MIS-9 (340 ka), the Purple MIS-11(445 ka) and the Green MIS-13 (570 ka) transitions (Grall et al., in press b). We adopt this colour code, denoting by these colours the sequence on top of the sequence boundary. In this paper we designate our own figures with a capital F as Fig. and figures we cite from the liturature with a lower case f as fig.

THE EASTERN SECTOR

Fig. 6 illustrates the faults we have mapped and Fig. 5A shows the locations of the multichannel seismic profiles that were used to identify them. Fig. 6 shows the eastern sector of our study area consisting essentially of the Çınarcık Basin (Le Pichon et al., 2001; Ateş et al., 2003; Carton, 2005; Şengör et al., 2005; Laigle et al., 2008; Uçarkuş, 2010) and regions to its north (Gökçeoğlu et al., 2009; Özeren et al., 2010; for the neotectonics of the land area see Şengör, 2011) and south (including the İmralı Basin: Okay et al., 2000; Sorlien et al., 2012). Çınarcık Basin is a critical area because the exact manner of the westward prolongation of the faults from it to the Central High remains unclear.

154 In this sector we have chosen profiles 9 (Fig. 7) and 13 (Fig. 8) to illustrate the relative
155 age sequence of the faults (for locations of the profiles, see Fig. 5A). Fig. 7 shows that
156 along the profile 9, the main marginal fault cuts to the surface. The seismicity also
157 shows it to be active localising almost exclusively right-lateral earthquakes (Figs. 6B and
158 C; Örgülü and Aktar, 2001; Özalaybey et al., 2002, 2003; Pınar et al., 2003). In Fig. 6, the
159 focal mechanism solution 44 is not readily interpretable in terms of simple shear zone
160 geometry, but it is still compatible with a tension gash orientation, albeit with a tiny
161 sinistral component. We note that the term 'tension gash' is here used to denote a
162 *structure orientation as seen in micro-and meso-scales, where the structure was originally*
163 *liquid-filled*. The structures we describe are not necessarily 'tensional' but definitely
164 'extensional' with variable amounts of strike-slip associated with them (from 0% to 50%
165 in some rare cases). As we have not read the seismograms ourselves we cannot further
166 comment on that solution. If it is a 'tension gash' orientation normal fault only, then it
167 is also compatible with pure strike-slip along the northern margin of the Çınarcık Basin.

168 The entire sedimentary fill seen in this basin is of Pleistocene age: In gravity core 27 (for
169 location, see Fig. 7B), a radiocarbon age of 16.1 to 16.5 ky BP Cal. was obtained at a
170 depth of 25 metres. In core 25, closer to the main bounding fault to the north, two ages
171 of 14.3-16 and 15.0-16.5 ky BP Cal. were obtained from depths of 28 and 32 metres,
172 respectively (Beck et al., 2007). They indicate a mean sedimentation rate of 1.5-2 mm/a
173 during the Holocene within this basin. These ages make the entire sedimentary section

as seen in Fig. 7 Pleistocene in age (Şengör et al., 2005) with the exception of the first 15 to at most 20 metres from the sea-floor, which represent Holocene sedimentation.

The fault to the south of the main fault in this profile (Fig. 7) cuts only up into a low amplitude layer at around 1.5 s twt, but does not penetrate farther up. On the evidence of the seismic profile that fault seems to have died within the Pleistocene (since 540-450 ka). Neither is that any evidence of its presence in the Chirp profile published by Zitter et al. (2012). However, there is seismicity correspondent to its location and available fault-plane solutions associated with that seismicity (solutions 33, 36, 39 in Fig. 6C) all indicate dextral strike-slip; the fault-plane solution 36 indicates a very slight extensional component either on a dextral Riedel shear (R) or on a sinistral anti-Riedel (R') shear, both entirely compatible with the main shear zone (the Y-shear direction) being a right-lateral one (see Fig. 9 for the terminology we use for various shear zone structures). These earthquakes indicate a non-negligible strain being taken up on the fault that on the seismic profile 9 does not seem to reach the surface. The earthquakes' magnitudes are small enough and the data of the multichannel seismic profiles are coarse enough that the sea bottom's either not being breached or appearing not to have been breached is entirely understandable. That the fault does not show up even on the Marnaut 54 Chirp profile (Zitter et al., 2012) may suggest that in levels shallower than the green sequence the fault may branch out and even merge with the main boundary fault and reaches the surface via that route.

194 A south dipping fold and trust along the southern margin of the Çınarcık Basin
195 separated two small basinal structures (Fig. 7 and Fig. 5B). Farther east there is an Ms
196 6.4 earthquake that gave a normal fault solution (solution labelled T in Fig. 7C: Taymaz
197 et al., 1991) where shallow transtensive faults could be mapped on both bathymetry and
198 chirp sub-bottom profiles, corroborating the view that at least some of the faults in this
199 set are active (Fig. 5B). The microearthquake activity along these southern normal faults
200 seems livelier than in the north since 2005, but the southern normal faults do not
201 generate as large earthquakes as the northern main strike-slip strand, which is what is
202 expected from their respective rates of motion (see Şengör et al., 2005).

203 Within the Çınarcık Basin, the northern master fault takes up by the largest portion of
204 the movement which is nearly perfectly parallel with it as seen both from the
205 earthquake fault plane solutions and from the GPS data (see Şengör et al., 2005 for a
206 summary of the GPS vectors here) and there is no indication of major oblique-slip,
207 contary to what is implied by Seeber et al. (2006), who over-estimated the oblique-slip
208 component at the crustal level, as they did not take into account the compaction, which
209 in a mature basin, could result in a seafloor subsidence 2 to 3 times larger than the
210 subsidence of the basement. We have not taken into account in our study Hergert and
211 Heidbach's (2010) modelling of the mechanical behaviour of the lithosphere in the
212 Marmara Region which requires derivation of stresses. Such a derivation is hardly
213 possible (except in a model), given the uncertainties concerning the properties of the

real lithosphere and the stresses acting in it, but if one wished to invoke that model, the northern margin of the Çınarcık Basin would still require less than 4.5 mm/yr normal component of motion within its constraints, which we find reassuring.

Farther south, west of the Armutlu Peninsula, there is the southerly-to-southeasterly-tilted İmralı Basin (Okay et al., 2000), also of Pleistocene age. Microearthquake activity (Fig. 6B and C) is much subdued here, only a few events falling directly on the profile. This shows that even the ~~'inactive'~~ faults probably move, albeit rarely, during small magnitude earthquakes, but contribute essentially nothing to the further straining of the area. Along its easterly strike continuation, on the Samanlı Mountains (for their detailed geomorphology, see Bilgin, 1967), there is a livelier earthquake activity. The fault plane solutions available from there readily fall into two groups: a western group (fault plane solutions 16, 45, 47, 49, 51 in Fig. 6C) and an eastern group (solutions 53 and 54). It seems that the western group faults stretch the ground in a NNE-SSW direction and are related to those that created the İmralı Basin and the ones farther east cause extension in a NE-SW direction and are associated with the fault family that caused the Ms=6.4 Çınarcık earthquake farther north. Within the İmralı Basin, the main faults strike WNW-ESE and are related to the faults that cause the western group of earthquakes in the neighbouring Samanlı Mountains. But they are probably not mainly responsible for the origin of the İmralı Basin. Otherwise, the neighbouring Samanlı Mountains with similar and active faults would not have stood as high as they do now.

Fig. 8A shows profile 13 which is farther west than the previous one (Fig. 7A) and Fig 8B our interpretation of it. The recognisable sequences indicate a much narrower basin of a similar age to the one we saw farther east. Although this sub-basin is bounded by faults that cut to the sea-floor there is one between them that is much older, possibly pre-Pleistocene. The southerly-tilted basin here appears completely inactive, as none of the faults that appear related to its formation cut to the surface. The spread of microseismicity (Figs. 6B and C) corroborates this picture showing only a few scattered epicentres.

Sorlien et al. (2012) have presented a meticulous and exhaustive analysis of the seismic stratigraphy of the Imrali Basin fill with a view to establishing a chronostratigraphy that they then used to argue that faulting continued at a constant rate since about half a million years ago. This is based on the date of what they call the red horizon, which has been correlated other most of the Sea of Marmara and has been attributed an age of 109 ka based on extrapolation from Marion-Dufresne cores (Sorlien et al., 2012; Grall et al., in press b). Lower reflectors have been correlated to low stand deltas and age attributed with the assumption that the sediment input into the Imrali basin has been of the same order for each glacial cycle. However, this reasoning also led to the conclusion that the low-stand delta observed in stratigraphic succession do not systematically correspond to successive glacial cycles. In the absence of independent age constraints, ambiguities in the age attributions thus cannot be resolved. In detail, Sorlien et al. (2012) age model

254 taken as face value does suggest some slowing down of the subsidence over the last 130
255 to 330 ka once compaction is taken into account. In both profiles it is difficult to
256 ascertain whether the basin fill of the Çınarcık and the İmralı basins is conformable or
257 unconformable with their stratigraphic basement. Because at least one fault is truncated
258 by the bottom sequence (Fig. 8B) and some reflectors below the lowest sequence seem to
259 have a geometry in places not exactly parallel with the basement layering, we assume
260 an unconformity bounding the basin at the bottom, which is, however, not easy to
261 defend conclusively on the basis of the available observations.

262 Interestingly, once one goes southward over the Samanlı Mountains on the Armutlu
263 Peninsula (SA in Fig. 5A), the microseismicity again becomes lively in the Gulf of
264 Gemlik (GG in Fig. 5A). A major fault strand, which we here term the Gemlik-Bandırma
265 Fault, goes from there to the Erdek tombolo (ET in Fig. 5) and then turns
266 southwestward in the county Gönen into the Biga Peninsula (Fig. 5). Young scarps all
267 along the fault suggest recent activity and at least two estimated M=7 earthquakes (128
268 and 543 CE) seem to have taken place on it during historical times (Fig. 4). Kuşçu et al.
269 (2009) mapped a group of active faults in the Gulf of Gemlik and microearthquakes
270 align along smaller faults on the isthmus separating Lake İznik and the Gulf of Gemlik,
271 all betraying a lively activity although not accomplishing much strain (no earthquakes
272 above magnitude 4), except obviously at intervals of a minimum or a millennium-and-
273 a-half. Although Barka and Kadinsky-Cade (1988) called it the 'middle branch of the

North Anatolian Fault', it is much less significant than the two major strands originally identified by Dewey and Şengör (1979) and Şengör (1979) and is not much different from the many deactivated faults populating the broad southern shelf of the Sea of Marmara (Fig. 5A). Therefore, we go along the recent trend in following Dewey and Şengör (1979) and Şengör (1979) and stick to two major strands, but we nevertheless point out that the Gemlik-Bandırma fault does maintain an activity, although much subdued.

THE CENTRAL SECTOR

This sector (Fig. 10), as herein used, corresponds mostly to what is called the Central High in the literature (it is the high region that completely surrounds the Kumburgaz Basin, KB; Le Pichon et al., 2001; Şengör et al., 2005) but that also includes the Kumburgaz Basin and almost the whole of the Central Basin (Le Pichon et al., 2001; Şengör et al., 2005). The presence of the Kumburgaz Basin atop the Central High provides a sediment receptacle and thus a welcome means to date the faults cutting the Central High relative to one another (see especially Sorlien et al., 2012, fig. 6).

Profile 23 (Fig. 11A and B) is located in the eastern and central part of the basin and shows that both its bounding faults there cut to the surface (Fig. 11B). The basin also has other faults in it, but they seem to have died shortly after the basin initially formed. We also see that the basin was initially narrower. However, the faults that bound the basin on this profile are not parts of a single fault family: the northern fault is along the strike

294 of the northern boundary fault of the Çınarcık Basin coming from the east, here forming
295 a part of the main zone of displacement along the northern branch of the North
296 Anatolian Fault (Şengör et a., 2005). The southern fault, however, has an WNW strike
297 and seems to be a somewhat rotated, extensional Riedel shear so identified simply on
298 account of its orientation. Immediately to its south there is another fault similar to it that
299 also bounds the basin. Both of these faults cut to the surface and both are active as
300 shown by the microseismicity they localise. To their east, the southern basin margin
301 seems unfaulted as can be seen on fig. 6 by Sorlien et al. (2012). Sorlien et al. (2012) carry
302 what they call the Red-1 reflection into the Kumburgaz Basin where it is clearly cut
303 twice, whereas in the İmralı Basin it is not, where it records the lower boundary of a
304 non-faulted floor of a sedimentary infill. Therefore, although a throughgoing main
305 strike-slip fault appears to have already formed in the Kumburgaz Basin, the auxiliary
306 faults, such as the two Riedels just mentioned, appear not to have not terminated their
307 activity. They probably do not localise major shocks (no earthquakes above magnitude
308 4) and therefore do not take up much displacement, but they nevertheless remain active
309 and it is hard to tell up to what size earthquakes they might one day localise.

310 Profile 27 (Fig. 12A and B) shows a much wider basin, of almost bovine-head shape
311 when considered together with the narrower fault trough underlying it, and numerous
312 faults cut its most recent sequence. Although the major displacement is along the
313 northern master fault bounding all the sequences and reaching the sea-floor, it seems

314 that during the deposition of the youngest sequence, the basin had already become
315 much wider. The numerous faults to the south, sub-parallel with the two previously-
316 mentioned Riedel shears, are all either active or terminated their activity very recently
317 during the deposition of the top sequence. Many of these faults seem to be short,
318 therefore insignificant, in terms of the displacement they can accomplish, but they
319 nevertheless are mostly active.

320 When we look farther south, an active fault that strikes about N45°W, thus in an
321 extensional orientation in the overall North Anatolian Shear Zone, is seen to be active
322 with microearthquake epicentres on it. Yet it sits perfectly on strike with, and seems to
323 be the northwesterly continuation of, a major inactive fault extending down into the
324 Gulf of Gemlik.

325 Oblique (N120°-N140°) transtensional blind and deep-seated faults, identified in the
326 western part of the Sea of Marmara, are part of a northeast dipping extensional fault
327 system named the South Transtensional Zone (STZ) by Grall et al. (2012). Many of
328 these faults appear still active, although we do not know what portion of the total shear
329 they accommodate. In particular, the western part of this fault system is suspected to
330 play a rôle in the landslide activity in the Ganos area (in our western sector: Zitter et al.,
331 2012). The long fault mentioned in the previous paragraph is the partly active eastward
332 termination of this transtensional system providing a connection between the main
333 northern branch of the North Anatolian Fault and the fault system to the south recently

named the Southern Marmara Fault by Le Pichon et al. (in press). ~N100° striking, mainly wrench faults occur also in the eastern part of the Sea. These faults, which may be blind, are probably a part of the Central Fault System (CFS, Grall et al., 2012). Other, shorter, faults close to and parallel with the inactive strand are, by contrast, still active. A small family of short faults with the same orientation to the east of the meandering submarine canyon seen in Fig. 10C are all active and clearly localise microearthquakes. By contrast, some abutting against the bounding faults of the spindle-shaped basin within the Central Basin appear dead, perhaps because they have been recently decapitated by the main northern branch of the North Anatolian Fault. All of the faults belonging to Grall et al.'s Central Fault System belong to the tension-gash-orientation (refer to Fig. 9 to see what that orientation means) normal faults related to the North Anatolian Shear Zone.

Curiously, the longer E-W orientated faults along Y-shear directions (cf. Fig. 9), some turning into Riedel and P-shear orientations at their ends, seem in some segments active and in others inactive.

Farther west, within the Central Basin, the microearthquake activity shows that the smaller spindle-shaped basin within the Central Basin is where most of the present activiy is located, but the northeastern border of the larger basin is also active (Figs. 10 B and C). The active, spindle-shaped basin within the larger Central Basin is in fact where the Holocene subsidence rate is the highest in the Sea of Marmara (reaching more than 7

mm/a, Grall et al., 2012). This centralised subsidence is in stark contrast to the situation encountered in the Çınarcık and the Kumburgaz basins, where the main displacement zone is along the northern master faults of the basins.

So far, we had encountered no active faults in a shortening orientation. We encounter such a fault for the first time here, along the main displacement zone of the North Anatolian Fault in the Sea of Marmara just east of the Central Basin where the main strand is connected to the small spindle-shaped basinette in the middle of the Central Basin (Fig. 10B).

Within the southern Marmara Shelf, the available seismic profiles show that all the faults terminated their major movement at the end of the early Pliocene (3.5 Ma), but there is sparse, broadly spread microseismicity (Le Pichon et al., in press).

THE WESTERN SECTOR

The western sector (Fig. 13) houses what is termed the Western High and the Tekirdağ (ancient Rodosto) Basin. We selected two profiles to show here, one across the High (profile 70: Fig. 14A and B) and another, across the Basin (profile 78: fig. 16A and B).

Profile 70 (Fig. 14A) shows a much-faulted anticlinal ridge rising in the deepest part of a trough-shaped basin that is not seriously faulted at either end. Although what faults there are dip towards the basin, their vertical displacements are insignificant compared with the marginal faults of the Çınarcık, Kumburgaz and the Central basins. The basin

in fact has the appearance of a sag in the midst of which the peculiar anticlinal ridge of the Western High rises. It seems that the only active faults are those that bound the Western High, the southern with a higher rate of vertical motion as judged from the thickness of the green sequence. It is that fault which coincides with the main displacement zone of the northern branch of the North Anatolian Fault here. Some of the faults that cut the high are active, others dead and yet both dead and active faults seem to belong to the same set of steep thrusts. This is another region where we see active faults in a thrust orientation. In fact, the entire geometry of the Western High, with its flanking basins, gives the impression of a shortening structure that originally consisted of a broad synclinal basin, in the middle of which an anticline later rose. This is also supported by the topography of the sediment/acoustic basement interface, which reveals a deep trough which extends from the Central Basin towards the east and to the Tekirdağ Basin towards the West, such as Bayraçkı et al. (in press) recently depicted. It seems that the throughgoing faulting chose the anticline to follow and in so doing sliced it with small and steep thrusts.

We have no data as to the nature of the sequences seen in the seismic profiles across the Western High making up its foundation. It is however very likely that they consist of the Ganos Flysch wedge that delimits the Thrace Basin to the south and the Mio-Pliocene gently-dipping sedimentary rocks covering the flysch wedge as one sees on the Gallipoli Peninsula, where even deeper portions of the accretionary wedge crop out

(e.g., Şentürk and Okay, 1984 report blueschists that crop out from under the flysch and the surrounding younger Cainozoic rocks)

The second profile, 78 (Fig. 15), goes across the Tekirdağ Basin. In principle it shows the same structures that one sees in the Western High, except the central anticline is here asymmetric and north-vergent, delimited against the northern, deeper half of the basin by a very steep, essentially vertical fault. Okay et al. (1999) interpreted it as a south-vergent thrust, which is contrary to what is seen along profile 78 (Fig. 15A). The southern part of the anticline is not broken by faults (except two very shallow landslide faults) but has the form of a syncline. The sequences betray a faster subsidence in the basin centre than along its sides consistent with the syncline interpretation.

The steep fault is a continuation westwards of the main displacement zone. The smaller large fault to the north achieves not much of a vertical displacement and seems a part of a series of short, *en-échelon* faults that seem an abortive attempt to reach the northern end of the Ganos (MG in Fig. 13A) constraining bend thrust zone (Dewey and Şengör, 1979; Şengör, 1979; see Fig. 18 herein) by tearing a strike-slip fault from the northern basin north of the Western High across the northern part of the Tekirdağ Basin. That attempt seems to have been abandoned, however, while the youngest sequence was being deposited. There is essentially no microseismic activity along that trend of small faults.

Two other short trends of faults on the basin floor to the east of the middle part of the

Ganos constraining bend suggest other attempts at reaching it farther north than its present southernmost end. Although both attempts seem to have failed, the latter group of faults are still active as indicated by a lively microseismic activity at their eastern ends, but this is probably because of the loading of the crust in which they reside by the Ganos Wedge (see Fig. 16 for the cross-sectional geometry of the Ganos overthrust zone along the restraining bend).

At the latitude of the Western segment, seismic activity on the South Marmara Shelf is considerably livelier than in the Central Segment. Here we have in fact four earthquakes with magnitudes larger than 6 (Fig. 17) on the Biga Peninsula, the western continuation of the southernmost part of the South Marmara Shelf. The microearthquake activity is also much higher than it is in the Central Sector.

In this sector, the Marmara Island (the ancient Proconnesos: the largest island in Fig. 17) is a divider: to the east nearly all major faults strike W to NW; to its west nearly all strike NE, indicating that the shear zone takes a fairly sharp bend to the southwest with accompanying appearance of major thrust earthquakes along the fault segments. The faults also acquire here a much greater continuity than they have in the east, as one would expect from thrust faults as opposed to normal faults which are numerous east of the Marmara Island. Interestingly, west of the Marmara Island all the major strands are active, presumably because here the 2.5 cm/a motion of the Marmara Block delimited by the northern and the southern strands of the North Anatolian Fault (Le

433 Pichon et al. 2003) must be compensated in part by shortening and it is more economic
434 to distribute the shortening and consequent crustal thickening on many faults.
435 However, here too the strike-slip faults display their characteristic complex strains by
436 localising earthquakes of all three kinds of fault types (Fig. 17)!

437 DISCUSSION

438 *Temporal evolution of the North Anatolian Fault in the Sea of Marmara*

439 When we started this study, we were expecting, as expressed in Şengör et al. (2005), an
440 orderly evolution of a shear belt in which an initially broad shear zone characterised by
441 such 'secondary' or 'auxiliary structures' as Riedel (R) and Anti-Riedel (R') shears, X,
442 and P shears and tension gashes (T) with shortening structures(S) gradually evolving
443 and eventually abandoning the field of deformation to a narrow thorough-going fault
444 consisting of segments of Y shears, much as in the experiments of Riedel (1929),
445 Tchalenko (1970), Wilcox et al. (1973), Bartlett et al. (1981), Naylor et al. (1986) and
446 Ahlgren (2001) and as depicted in our Fig. 9. What we have found instead is a much
447 more haphazard development. If one separates the fault families expected from the
448 experiments into R, R', X, P and Y shears and T and S structures according to their
449 orientations and, wherever available, from earthquake first-motion solutions and
450 stratigraphic vertical separations and note their sequence of occurrence in the analogue
451 experiments as R', R, P, X and, if the material being sheared is suitable to form them,
452 first S and then T structures, Nature shows us that in the Sea of Marmara almost all of

453 these structure types are active now. We have actually seen no X shears that can be
454 confidently identified and some of the fault segments bending into a P-shear orientation
455 are all now dead. What is even more peculiar is the observation that some faults may
456 have both dead and active segments along them (within the time frame of a part of the
457 Pleistocene, mostly even late Pleistocene-Holocene)! An extreme example has been
458 recently documented by Le Pichon et al. (in press), who showed that what they called a
459 South Marmara Fault under the late Pliocene beds in the South Marmara Shelf appears
460 entirely inactive there at least for the last 2.5 or 2.6 Ma, yet both at its eastern and
461 western ends it is today active! Kuşçu et al. (2009) showed that the faults in the Gulf of
462 Gemlik are active and the prolongation of the South Marmara Fault into the Aegean in
463 the west just localised a Mw 6.2 dextral slip earthquake on 8th January 2013 (Le Pichon
464 et al., in press)! This suggests that some dead fault strands may be connected to active
465 ones by as yet unrecognised intermediate segments.

466 An extremely interesting observation has been reported recently by Shillington et al.
467 (2012): they showed the presence of folds forming by downslope creep on steep (3^{o} to
468 10^{o}) slopes in and around the main trough of the Sea of Marmara. Interestingly, with the
469 exception of the slope north of the Armutlu Peninsula and to the south of the Central
470 Basin, all of the slopes on which such creep folds have formed and in places continue to
471 form are on the slopes of structures that are in a shortening orientation and have been
472 so since the shear began. The Çınarcık exception is easy to explain in terms of the active

473 normal faulting going on at the foot of the Armutlu Peninsula. The slope south of the
474 Central Basin may have been accentuated by the faults that there exist along the South
475 Marmara Shelf (see Le Pichon et al., in press), but the data there are not adequate to
476 address this question. Shillington et al.'s (2012) work is a very nice possible example of
477 structures forming concurrently with growing folds on a large scale, perhaps not
478 dissimilar to the situation as documented by the progressive growth in time (late
479 Cretaceous to Eocene) of the Hathira (Makhtesh-Hagadol or Kurnub) anticline in
480 southern Israel (Eyal, 2011).

481 Although most of the elements of the shear zone in the Sea of Marmara are active now,
482 the strain they accomplish is extremely variable. It seems that almost all the motion of
483 the Eurasia/Marmara Block (the area delimited by the northern and the southern
484 strands of the North Anatolian Fault: Le Pichon et al., 2003) is taken up by the Y-shears
485 making up what Le Pichon et al. (2001) and Şengör et al. (2005) termed the main
486 displacement zone forming, from east to west, the main northern bounding faults of the
487 Çınarcık and the Kumburgaz basins, the fault cutting through the Central Basin and
488 bounding the small spindle-shaped basin in the middle, and the fault delimiting the
489 Western High and the Tekirdağ Basin to their south. All other active faults seem to cut
490 to the sea-floor and nucleate microseismic shocks with few exceptions, such as the
491 normal faults south of the Çınarcık Basin that nucleated an Ms=6.4 earthquake and
492 possibly another one in 1894 that greatly damaged İstanbul. They contribute very little

493 to the overall strain, yet Le Pichon et al. (2003) documented that the small strain was by
494 no means negligible and is detectable by GPS observations. However, Sorlien et al.'s
495 (2012) thesis that the faults have moved with a constant rate during the last half a
496 million years, which implies in view of the ~ 55 km total offset for the entire Marmara
497 area (Akbayram and Okay, 2012; Şengör et al., 2005) that the Sea of Marmara has a total
498 history of less than half a million years, which is certainly incorrect.

499 The difference between the experiments and Nature as it appears to us in the
500 neotectonics of the Marmara region may be twofold: one is the time scale. What
501 happens in nature in thousands to hundreds of thousands and even a couple of million
502 years, happens in experiments in a matter of minutes or at most hours. We may be
503 seeing a process of slow demise of the auxiliaries in Nature, which to us seem a time of
504 activity in concert. In reality, the auxiliaries may be slowly passing away as the main
505 displacement zone gathers the action onto itself. The fact that nearly all the main
506 displacement today is concentrated on the almost completely throughgoing main
507 displacement zone may be a result of its gradual climb to prominence, a climb that has
508 not yet reached the summit.

509 The second difference pertains to the extreme heterogeneity of the natural material
510 which the shear zone deforms as opposed to the nearly homogeneous materials used in
511 the experiments. No experiment can hope to reproduce the multifarious natures of the
512 materials making up the area in and around the Sea of Marmara. Entire domains

513 consisting of very different types of materials dominate the Marmara area and the
514 developing shear zone no doubt exploited every bimaterial surface to break through on
515 all sorts of scales. That is mainly why we have been unable to use with confidence the
516 kind of modelling represented by Hergert and Heidbach's (2011) paper, where rock
517 properties in the sedimentary carapace are accepted to be distributed homogeneously—
518 which is manifestly not the case, if for no other reason than the depth differences among
519 basin basements, even within a single basin—and the great variations in the rock
520 properties in the basement are not even considered. Şengör et al. (2005) pointed out that
521 the North Anatolian Fault as a whole seems to have nucleated along the northern 'wall'
522 of the Tethyside accretionary complexes against the more indurated basement of the
523 Rhodope-Pontide Fragment (see Fig. 2), very much corroborating the theoretical model
524 of Ben Zion and Andrews (1998) and Ben Zion (2001). There is little doubt that the
525 sensitivity of bimaterial surfaces to preferentially produce rupture under stress is also
526 present at much smaller scales between the tectonic units made up of different materials
527 under and around the Sea of Marmara and between different rock packages within
528 those tectonic units.

529 *The origin of the Marmara Deeps*

530 Both the Western and the Central Highs have east-northeasterly trends. Fig. 14A
531 shows the Western High having an overall anticlinal structure albeit sliced by
532 numerous faults. We had originally hypothesised that the anticline was a function of

533 the shear evolution and asked ourselves that if we reverse the shear along the North
534 Anatolian Shear Zone, what orientation the high would acquire. Our expectation was
535 that it would rotate into a more northeasterly direction and we expected a similar result
536 from the Central High. Fig. 18A shows the present day fault geometry within the Sea of
537 Marmara and the outlines of the two highs in blue. Fig. 18B shows the situation if a
538 homogeneous strain is imposed on the system to reverse a 55 km offset. Because the
539 overall ofset along the North Anatolian Shear Zone is 75 to 80 km along its entire length
540 (Şengör et al., 2005), we subtracted the offset of some 26 km seen along the Pamukova
541 strand leading to the main southern strand (Şengör et al., 2005) from that to obtain the
542 55 km left-lateral offset on the entire Sea of Marmara fault family to reverse the present
543 right lateral shear for the purposes of Fig. 18. This seems consistent with the 52 km
544 offset reported by Akbayram and Okay (2012) from the northern strand east of the Sea
545 of Marmara. The timing of the offset reported by Akbayram and Okay (2012) is
546 problematic, however, because some of it could have formed just after the medial
547 Eocene collision along the Intra-Pontide suture in a completely different system of
548 strike-slip faults (Akbayram et al., 2013). It is clear, however, that at least the Marmara
549 Fault family north of the South Marmara Shelf takes up a displacement that farther east
550 is concentrated on the northern strand of the North Anatolian Fault and that offset is an
551 absolute maximum of 57 km. Fig. 18C shows what is seen when we superimpose Figs.
552 18A and 18B keeping the northern boundary fixed. *The highs do not rotate as we expected,*
553 *but acquire a lumpier appearance*! In fact, as a result, they present an optical illusion as if

554 they rotated into a more E-W orientation when the displacement is reversed.

555 This to us suggests that the highs, or their much more subdued forerunners, were
556 probably there before the shear began and were similar to gentle axial culminations
557 along outer arc highs in present-day forearcs, in this case possibly either accentuated or
558 even initially caused by the collision. When the shear began they were shortened into S
559 structures and became elongated in an ENE orientation. The Western High was
560 probably only a gentle 'suggestion' with a broad basin, a simple 'undulation,' of the
561 basin floor, which later became accentuated as the shear evolved. The fig. 6 in Sorlien et
562 al. (2012) very nicely shows the anticlinal structure of the Central High and the smaller
563 wavelength folds right across it involving even the youngest sediments, although there
564 is a clear decrease in folding amplitude up section (the reverse of what one sees in the
565 so-called 'generative folds'; our sorts of folds may thus be called 'degenerative')
566 indicating a waning of the shortening commensurate with the concentration of the
567 shear along the northern branch of the North Anatolian Fault.

568 The Çınarcık Basin is clearly not a part of this system as indeed it does not sit in front of
569 the Thracian fore-arc basin, but in front of the more solid and homogeneous İstanbul
570 Zone (Şengör 2011, fig. 1) and in a totally different orientation, *viz* WNW. We think that
571 the interpretation of it by Uçarkuş (2010) as a fault wedge basin *sensu* Crowell (1974) is
572 so far the best explanation for the origin and the present structure of the basin, so we do
573 not further elaborate on it here, except to say that it is a completely different sort of

574 basin from the other, more westerly, basins of the Sea of Marmara.

575 *The offset along the northern branch of the North Anatolian Fault*

576 Fig. 18 C further shows that the statement by Le Pichon et al. (2001) that the offset along
577 the very young northern branch of the North Anatolian Fault, at least west of the
578 Çınarcık Basin, is only some 4 km, falls out of the distributed shear interpretation. If the
579 shear has been really as distributed as the Fig. 18 approximates, then the offset along
580 the level of the Central Basin/Western High comes to at most 5 km. and no more.
581 Therefore, the fault families we have mapped in the Sea of Marmara must have initially
582 taken up the entire displacement that falls to the share of the present-day Northern
583 Branch altogether. That many of them are still active (although probably dying)
584 corroborates this view. That the South Marmara Shelf fault families are almost all dead
585 (with the exception of the present microseismic activiy), but that more activity is seen in
586 the northern auxiliary structures, on both seismic and stratigraphic (Sorlien et al., 2012)
587 evidence, may be an indication of the fact that the displacement is gradually gathering
588 itself to the northern branch alone.

589 CONCLUSIONS

590 The present day fault families younger than about the medial Miocene in the Sea of
591 Marmara are all parts of the North Anatolian Shear Zone and they all seem to have
592 shared among themselves a total offset of some 55 km along this zone since the later

593 medial Miocene. Contrary to expectation from analogue claycake and sandbox
594 experiments, a regular development from distributed structures to a single,
595 throughgoing strand cannot now be established, but this may be more a function of the
596 vastly different time-scales between the experiments and Nature herself than a
597 fundamental difference in the evolutionary sequence. That the Southern Shelf fault
598 family is now dead and that no major earthquake seems to be nucleated on the
599 auxiliaries (except in the southern part of the Çınarcık Basin) may indicate a gradual
600 localisation of the offset along the single strand of the Northern Brach of the North
601 Anatolian Fault.

602 This study gives support to the older ideas that intracontinental transform faults begin
603 their lives as broad shear zones and become gradually converted into single- (or at most
604 a few-) strand structures. What such a broad shear zone at depth looks like may be
605 displayed by the 15-km wide mylonite zone seen along the giant Irtysh shear zone
606 (displacement ≈ 2000 km) in Central Asia (Şengör and Natal'in, 1996). The numerous
607 active fault zones we see at the surface no doubt broaden with depth (earthquake
608 hypocentres are hardly deeper than some 10 km under the Sea of Marmara; below that
609 the deformation is most likely ductile) and given their density at the surface, they most
610 likely coalesce into a very broad ductile shear zone. Le Pichon et al.'s (2003) study has
611 corroborated the presence of such a general, distributed deformation south of the
612 Northern Branch of the North Anatolian Fault.

Fig. 19 shows a situation where the faults depicted on Fig. 18A have been widened to shear zones of some 4 km width, the presumed with of the San Andreas Fault below 10 km (e.g., McBride and Brown, 1986). In these regions of amphibolite grade metamorphism what a shear zone looks like is shown in the inset from the Diancan Shang late Cainozoic metamorphic shear zone Ailao-Shan along the Red River strike-slip fault in Southeast Asia (copied from Cao et al., 2011). We have flipped Cao et al.'s figure to make the shear right-lateral and the similarity of the hand sample to the map pattern displayed by the presumed depth-map of the Sea of Marmara fault family is staggering: it is one of the best examples of Pumpelly's rule that small structures mimic big structures and a further demonstration of Tchalenko's (1970) point that shear structures are independent of scale. . We thus think that at a depth below 10 km, the Sea of Marmara basement consists of sheared rocks of the kind seen below the Ailoa Shan strike-slip fault, which, by an interesting coincidence, is also nucleated on a suture zone bearing steep serpentinite screens (Şengör and Natal'in, 1996; Burchfiel and Chen, 2012, chapret 15, especially fig. 15-1). In deeply-eroded Precambrian terrains, the presence of such broad, vertical, anastomozing ductile shear zones are most likely expressions of large strike-slip faults at the surface, many of which were probably transform faults. As transform faults are dependable indicators of relative plate motion directions, this is one way to get a handle on such old plate motion directions.

ACKNOWLEDGEMENTS

633 This paper was written upon the invitation of Professor Ali Polat to whom we are
634 grateful for the honour of being included in a volume in memory of Tuzo Wilson.
635 Professor Namık Çağatay was a great source of knowledge and critique in all matters
636 stratigraphic. MARSITE funding made substantial parts of this study possible. All
637 marine work in the Sea of Marmara since 2000 forming the basis of this study was
638 undertaken with the active and cheerful support of the Turkish Navy. Detailed and
639 constructive reviews by Professors Kevin Burke and Mark Zoback substantially
640 improved the original presentation.

641 REFERENCES CITED

642 Ahlgren, S.G., 2001, The nucleation and evolution of Riedel shear-zones as deformation
643 bands in porous sandstone: J. Struct. Geol., 23, 1203–1214.

644 Akbayram, K., and Okay, A.I., 2012, The cumulative offset of North Anatolian Fault in
645 the Marmara region, northwest Turkey: EGU General Assembly, Vienna, Austria,
646 Abstract 240-2012.

647 Akbayram, K., Şengör, A. M. C. and Özcan, E., 2013, The evolution of the Intra - Pontide
648 suture: implications of the discovery of late Cretaceous – early Tertiary melanges:
649 Geological Society of America Abstracts with Programs. v. 45, no. 7, p. 672

650 Anderson, E. M., 1951. The dynamics of faulting and dyke formation with applications

651 to Britain, 2nd edition: Oliver and Boyd, Edinburgh and London, 206 pp.

652 Armijo, R., Pondard, N., Meyer, B., Uçarkuş, G., Mercier de Lépinay, B., Malavieille, J.,
653 Dominguez, S., Gustcher, M.-A., Schmidt, S., Beck, C., Çagatay, N., Çakir, Z., İmren, C.,
654 Eriş, K., Natalin, B., Özalaybey, S., Tolun, L., Lefèvre, I., Seeber, L., Gasperini, L.,
655 Rangin, C., Emre, O., Sarikavak, K., 2005, Submarine fault scarps in the Sea of Marmara
656 pullapart (North Anatolian Fault): implications for seismic hazard in Istanbul.
657 Geochemistry, Geophysics, Geosystems 6, Q06009. doi:10.1029/2004GC000896.

658 Ateş, A., Kayıran, T. and Sincer, İ., 2003, Structural interpretation of the Marmara
659 region, NW Turkey, from aeromagnetic, seismic and gravity data: Tectonophysics, v.
660 367, pp. 41-99

661 Barka A., 1992, The North Anatolian Fault zone: Annales Tectonicae v. 6, pp. 164–95

662 Barka A., 1996, Slip distribution along the North Anatolian Fault associated with the
663 large earthquakes of the period 1939 to 1967: Bulletin of the Seismological Society of
664 America, v. 86, pp.1238–1254

665 Barka, A.A., and Kadinsky-Cade, K., 1988, Strike-slip fault geometry in Turkey and its
666 influence on earthquake activity: Tectonics, 7/3, pp. 663-684.

667 Bartlett, W. L., Friedman, M. and Logan, J. M., 1981, Experimental folding and faulting
668 of rocks under confining pressure. Part IX. Wrench faults in limestone layers:

669 Tectonophysics v. 79, pp. 255 -277.

670 Bayrakçı, G. Laigle, M., Bécel, A., Hirn, A., Taymaz, T., Yolsal-Çevikbilen, S. and the
671 SEISMARMARA Team, 2013, 3-D basement tomography of the northern Marmara
672 trough by a dense OBS network at the nodes of a grid of controlled source profiles
673 along the North Anatolian Fault: Geophysical Journal International, v. 194, pp. 1335-
674 1357.

675 Bécel, A., 2006, Structure Sismique de la Faille Nord Anatolienne en Mer de Marmara:
676 École Doctorale des Sciences de la Terre, Institut de Physique du Globe de Paris, 286 pp.

677 Bécel, A., Laigle, M., de Voogd, B., Hirn, A., Taymaz, T., Yolsal-Çevikbilen, S.,
678 Shimamura, H., 2010, North Marmara Trough architecture of basin infill, basement and
679 faults, from PSDM reflection and OBS refraction seismics: Tectonophysics, v. 490, pp. 1-
680 14.

681 Beck, C., Mercier de Lépinay, B., Schneider, J.-L., Cremer, M., Çağatay, N.,
682 Wendenbaum, E., Boutareaud, S., Ménot, G., Schmidt, S., Weber, O., Eris, K., Armijo, R.,
683 Meyer, B., Pondard, N., Gutscher, M.-A., MARMARACORE Cruise Party, Turion, J.-L.,
684 Labeyrie, L., Cortijo, E., Gallet, Y., Bouqueral, H., Görür, N., Gervais, A., Castera, M.-H.,
685 Londeix, L., de Resseguier, A., Jaouen, A., 2007. Late Quaternary co-seismic
686 sedimentation in the Sea of Marmara's deep basins: Sedimentary Geology, v. 199, pp.
687 65-89

688 Ben-Zion Y. 2001. Dynamic ruptures in recent models of earthquake faults: J.Mech.
689 Phys. Solids, 49:2209–44.

690 Ben-Zion Y., and Andrews D. J., 1998, Properties and implications of dynamic rupture
691 along a material interface: Bull. Seismol. Soc. Am. 88:1085–94.

692 Bilgin, T., 1967, Samanlı Dağları—Coğrafî Etüd: İstanbul Üniversitesi Edebiyat Fakültesi
693 yayını No.: 1294, İstanbul Üniversitesi Coğrafya Enstitüsü Yayını No. 50, VIII+196 pp.

694 Burchfiel, B. C. and Chen, Z. L., 2012, Tectonics of the Southeastern Tibetan Plateau and
695 its Adjacent Foreland: Geological society of America Memoir 210, [iii]+231 pp.

696 Carton, H., 2005, Études Tectoniques en Mediterranée Orientale par Analyse de
697 Données de Sismique Réflexion: Mer de Marmara (Bassin de Çınarcık) et Marge du
698 Liban: École Doctorale des Sciences de la Terre, Institut de Physique du Globe de Paris,
699 Laboratoire de Géosciences Marines, 297 pp.

700 Carton, H., Singh, S. C., Hirn, A., Bazin, S., de Voogd, B., Vigner, A., Richolleau, A.,
701 Çetin, S., Ocakoğlu, N., Karakoç, F., Sevilgen, V., 2007, Seismic imaging of the three-
702 dimensional architecture of the Çinarcik Basin along the North Anatolian Fault: Journal
703 of Geophysical Research, v. 112, doi:10.1029/2006JB004548.

704 Cao, S., Neubauer, F., Liu, J., Genser, J., and Leiss, B., 2011, Exhumation of the Diancang
705 Shan metamorphic complex along the Ailao Shan-Red River belt, southwestern Yunnan,

706 China: Evidence from $^{40}Ar/^{39}Ar$ thermochronology: Journal of Asian Earth Sciences, 42,
707 525-550.

708 Çağatay, N., Wulf, S., Guichard, F., Özmaral, A., Sancar, Ü., Akçer-Ön, S., Henry, P. and
709 Gasperini, L., in press, Tephra record from the Sea of Marmara for the last 70 ka and its
710 paleoceanographic implications: American Geophysical Union, Fall Meeting 2013

711 Cormier, M.-H., Seeber, L., McHugh, C. M. G., Polonia, A., Çağatay, N., Emre, Ö.,
712 Gasperini, L., Görür, N., Bortoluzzi, G., Bonatti, E., Ryan, W.B. F., Newman, K. R., 2006,
713 North Anatolian Fault in the Gulf of Izmit (Turkey): rapid vertical motion in response to
714 minor bends of a nonvertical continental transform: Journal of Geophysical Research
715 111, B04102. doi:10.1029/2005JB003633.

716 Crowell, J.C., 1974, Origin of late Cenozoic basins in southern California: in Dickinson,
717 W. R., editor, Tectonics and Sedimentation, Spec. Publ. Soc. Econ. Paleont. Miner., 22,
718 pp. 190-204

719 Dewey, J. F., Hempton, M. R., Kidd, W. S. F., Şaroğlu, F. and Şengör, A. M. C., 1986,
720 Shortening of continental lithosphere: the neotectonics of Eastern Anatolia - a young
721 collision zone: in Coward, M.P. and Ries, A.C., editors, Collision Tectonics, Geological
722 Society of London Special Publication 19 (R.M. Shackleton volume), pp. 3-36.

723 Dewey, J.F., and Şengör, A.M.C., 1979. Aegean and surrounding regions: Complex

724 multiplate and continuum tectonics in a convergent zone: Geological Society of America
725 Bulletin, 90, pp. 84-92.

726 Dolu, E., Gökaşan, E., Meriç, E., Ergin, M., Görüm, T., Tur, H., Ecevitoğlu, B., Avşar, N.,
727 Görmüş, M., Batuk, F., Tok, B. and Çetin, O., 2007, Quaternary evolution of the Gulf of
728 Izmit (NW Turkey): A sedimentary basin under control of the North Anatolian Fault
729 Zone: Geo-Marine Letters , v. 27, pp. 355-381.

730 Ekström, G. and England, P., 1989, Seismic strain rates in regions of distributed
731 continental deformation: Journal of Geophysical Research, 94, B8, pp.10231-10257.

732 Eriş, K. K., Çağatay, N., Beck, C., Mercier de Lepinay, B., 2012, Late-Pleistocene to
733 Holocene sedimentary fills of the Çınarcık Basin of the Sea of Marmara: Sedimentary
734 Geology, v. 281, 151-165 pp.

735 Eyal, Y., 2011, The Syrian Arc Fold System: age and rate of folding: Geophysical
736 Research Abstracts, v. 13, EGU2011-7401, 2011 EGU General Assembly 2011.

737 Gasperini, L., Polonia, A., Del Bianco, F., Favali, P., Marinaro, G. and Etiope, G., 2012,
738 Cold seeps, active faults and the earthquake cycle along the North Anatolian Fault
739 system in the Sea of Marmara (NW Turkey): Bollettino di Geofisica Teorica ed
740 Applicata, v. 53, pp. 371-384.

741 Gazioğlu, C., Yücel, Z. Y., and Doğan, E., 2005, Morphological features of major

742 submarine landslides of Marmara Sea using multibeam data: Journal of Coastal
743 Research, v. 214, p. 664– 673

744 Géli, L., Henry, P., Zitter, T., Dupré, S., Tryon, M., Çağatay, M. N., Mercier de Lépinay,
745 B., Le Pichon, X., Şengör, A. M. C., Görür, N., Natalin, B., Uçarkuş, G., Özeren, S.,
746 Volker, D., Gasperini, L., Burnard, P., Bourlange, S. and the Marnaut Scientific Party,
747 2008, Gas emissions and active tectonics within the submerged section of the North
748 Anatolian Fault zone in the Sea of Marmara, Earth and Planetary Science Letters, 274,
749 34-39.

750 Gökçeoğlu C., Tunusluoğlu M. C., Görüm, T., Tur, H., Gökaşan, E., Tekkeli, A. B.,
751 Batuk, F. and Alp H., 2009, Description of dynamics of the Tuzla landslide and its
752 implications for further landslides in the northern slope and shelf of the Çınarcık basin
753 (Marmara Sea, Turkey), Engineering Geology , v. 106, pp. 133-153

754 Grall C., Henry P., Westbrook G.K., Cagatay M.N., Thomas Y., Marsset B., Bornschneck
755 D., Saritas H., Cifci G., Géli L.. Mass-Transport Deposits cyclicity related to glacial
756 cycles and marine-lacustrine transitions on the Sea of Marmara (Turkey) over the last
757 500 ka. in press a: Advances in Natural and Technological Hazards Research.

758 Grall C., Henry P., Tezcan D., Géli L., M. de Lepinay B., Rudkiewicz J-L, Zitter T.,
759 Harmegnies F., 2012, Heat flow in the Sea of Marmara Central Basin: Possible
760 implications for the tectonic evolution of the North Anatolian Fault. Geology,

761 10.1130/g32192.1

762 Grall C., Henry P., Thomas Y., Westbrook G.K., Cagatay M.N., Marsset B., Saritas H.,
763 Cifci G., Géli L. In press. Slip rate estimation along the western segment of the Main
764 Marmara Fault over the last 405-490 ka by correlating Mass Transport Deposits,
765 Tectonics, 10.1002/2012TC003255.

766 Herece, E. and Akay, E., 2003, Kuzey Anadolu Fayı (KAF) Atlası/Atlas of North
767 Anatolian Fault (NAF): Maden Tetkik ve Arama Genel Müdürlüğü, Özel Yayınlar Serisi
768 2, Ankara, [IV]+61 pp.+13 appendices as separate maps of 100,000 scale

769 Hergert, T. and Heidbach, O., 2011, Geomechanical model of the Marmara Sea region -
770 II. 3-D contemporary background stress field: Geophysical Journal International, v. 185,
771 pp. 1090-1102

772 Howell, F. C., Arsebük, G., Kuhn, S. L., Özbaşaran M. and Stiner, M. C., editors, 2010,
773 Culture and biology at a Crossroads: The Middle Pleistocene Record of Yarımburgaz
774 Cave (Thrace, Turkey): Ege Yayınları, İstanbul, xvi+[ii]+329 pp.+ 11+27 plates.

775 Ketin, İ., 1948. Über die tektonisch-mechanischen Folgerungen aus den großen
776 Anatolischen Erdbeben des letzten Dezenniums: Geol. Rundschau, 36, pp. 77-83.

777 Ketin, İ., 1969. Über die nordanatolische Horizontalverschiebung: Bulletin of the
778 Mineral Research and Exploration Institute of Turkey, 72, pp. 1-28.

779 Ketin, İ., 1976. San Andreas ve Kuzey Anadolu Fayları arasında bir karşılaştırma:
780 Türkiye Jeoloji Kurumu Bülteni, 19, pp. 149-154.

781 Kuşçu, İ., 2009, Cross-basin faulting and extinction of pull-apart basins in the Sea of

782 Marmara, NW Turkey: Turkish Journal of Earth Sciences v. 18, pp. 331–349.

783 Kuşçu, İ, Okamura M., Matsuoka, H., Yamamori, K., Awata, Y. and Özalp, S., 2009,
784 Recognition of active faults and stepover geometry in Femlik Bay, Sea of Marmara, NW
785 Turkey: Marine Geology, v. 260, pp. 90–101.

786 Laigle, M., Bécel, A., de Voogd, B., Hirn, A., Taymaz, T., Özalaybey, S., Çetin, S., Galvé,
787 A., Karabulut, H., Lépine, J. C., Saatçılar, R., Sapin, M., Shimamura, H., Murai, Y.,
788 Singh, S., Tan, O., Vigner, A. and Yolsal, S., 2008. A first deep seismic survey of the Sea
789 of Marmara: Deep basins and whole crust architecture and evolution. Earth and
790 Planetary Science Letters, v. 270, pp. 168-179

791 Le Pichon, X., Chamot-Rooke, N., Huchon. P., Luxey, P., 1993, Implications des
792 nouvelles mesures de géodésie spatiale en Grèce et en Turquie sur l'extrusion latérale
793 de l'Anatolie et de l'Egée. C.R. Acad. Sci. Ser. II 316:983–990

794 Le Pichon, X., Şengör, A.M.C., Demirbağ, E., Rangin, C., İmren, C., Armijo, R., Görür,
795 N., Çağatay, N., Mercier de Lepinay, B., Meyer, B., Saatçılar, R., and Tok, B., 2001, The
796 active Main Marmara Fault: Earth and Planetary Science Letters, 192/4, pp. 595-616.

797 Le Pichon, X., İmren, C., Rangin, C., Şengör, A.M.C., and Siyako, M., in press, The South
798 Marmara Fault, International Journal of Earth Sciences

799 Le Pichon, X. and Kreemer, C., 2010, The Miocene-to-Present Kinematic Evolution of the
800 Eastern Mediterranean and Middle East and Its Implications for Dynamics: Annual
801 Review of Earth and Planetary Sciences, v. 38, pp. 323-351.

802 Le Pichon, X., Şengör, A.M.C., Demirbağ, E., Rangin, C., İmren, C., Armijo, R., Görür,
803 N., Çağatay, N., Mercier de Lepinay, B., Meyer, B., Saatçılar, R., and Tok, B., 2001, The
804 active Main Marmara Fault: Earth and Planetary Science Letters, 192/4, pp. 595-616.

805 Le Pichon, X. and Kreemer, C., 2010, The Miocene-to-Present Kinematic Evolution of the
806 Eastern Mediterranean and Middle East and Its Implications for Dynamics: Annual
807 Review of Earth and Planetary Sciences, v. 38, pp. 323-351.

808 McBride, J.H., and Brown, L.D., 1986, Reanalysis of the cocorp deep seismic reflection
809 profile across the San Andreas fault, Parkfield, California, Bulletin of the Seismological
810 Society of America, 76, 6, pp. 1668-1686.

811 McKenzie, D. P., 1972, Active tectonics of the Mediterranean region: Geophysical
812 Journal of the Royal Astronomical Society, v. 30, pp.109–85.

813 McKenzie, D., Jackson, J., 1983, The relationship between strain rates, crustal thickening,
814 palaeomagnetism, finite strain and fault moments within a deforming zone: Earth and

815 Planetary Science Letters v. 65, pp. 182–202

816 Naylor, M.A., Mandl, G., and Supesteijn, C. H. K., 1986, Fault geometries in basement-
817 induced wrench faulting under different initial stress states: Journal of Structural
818 Geology, 8, 7, pp. 725-830.

819 Okay, A. İ., Kaşlılar-Özcan, A., İmren, C., Boztepe-Güney, A., Demirbağ, E. and Kuşçu,
820 İ., 2000, Active faults and evolving strike-slip basins in the Marmara Sea, northwest
821 Turkey: a multichannel seismic reflection study: Tectonophysics, v. 321, pp. 189-218

822 Okay, A.I., Demirbağ, E., Kurt, H., Okay, N., and Kuşçu, İ., 1999, An active, deep
823 marine strike-slip basin along the North Anatolian Fault in Turkey, Tectonics, 18/1, pp.
824 129-147.

825 Örgülü, G., and Aktar, M., 2001, Regional moment tensor inversion for strong
826 aftershocks of the August 17, 1999 İzmit earthquake (Mw=7.4), Geophysical Research
827 Letters, 28/2, pp. 371-374.

828 Özalaybey, S., Ergin, M., Aktar, M., Tapırdamaz, C., Biçmen, F., and Yörük, A., 2002,
829 The 1999 İzmit earthquake sequence in Turkey: seismological and tectonic aspects,
830 Bulletin of the Seismological Society of America, 92/1, pp. 376-386.

831 Özalaybey, S., Karabulut, H., Ergin, M., Aktar, M., Tapırdamaz, C., Biçmen, F., and
832 Yörük, A., 2003, Seismogenic zones of the Sea of Marmara: recent seismicity and focal

833 mechanism solutions, EGS-AGU-EUG Joint Assembly, 5, p. 12680, Nice, France.

834 Özeren, M. S., Çağatay, M. N., Postacıoğlu, N., Şengör, A. M. C., Görür, N. and Eriş, K.,
835 2010, Mathematical modeling of a potential tsunami associated with a late glacial
836 submarine landslide in the Sea of Marmara, Geo-Marine Letters, v. 30, pp. 523-539

837 Parke, J. R., Minshull, T. A., Anderson, G., White, R. S., McKenzie, D., Kuşçu, İ., Bull, J.
838 M., Görür, N. and Şengör, A. M. C., 1999, Active faults in the Sea of Marmara, western
839 Turkey, imaged by seismic reflection profiles: Terra Nova, v. 11, pp. 223-227.

840 Parke, J. R., White, R. S., McKenzie, D., Minshull, T. A., Bull, J. Kuşçu, İ., M., Görür, N.
841 and Şengör, A. M. C., 2002, Interaction between faulting and sedimentation in the Sea of
842 Marmara, western Turkey: Journal of Geophysical Research, v. 10.1029/2001JB000450

843 Pavoni, N., 1962, Die Nordanatolische Horizontalverschiebung: Geologische
844 Rundschau, v. 51, pp. 122-139.

845 Pinar, A., Kuge, K. and Honkura, Y., 2003, Moment tensor inversion of recent small to
846 moderate sized earthquakes: implications for seismic hazard on active tectonics beneath
847 the Sea of Marmara: Geophysical Journal International, v. 153, pp. 133–145.

848 Rangin, C., Le Pichon, X., Demirbağ, E. and İmren, C., 2004, Strain localization in the
849 Sea of Marmara: Propagation of the North Anatolian Fault in a now inactive pull-apart:
850 Tectonics, v. 23, TC2014, doi:10.1029/2002TC001437

851 Riedel, W., 1929, Zur Mechanik geologischer Brucherscheinungen, Centralbl. f. Mineral.
852 Geol. Pal., B, pp. 354-368.

853 Şaroğlu, F., 1985, Doğu Anadolu'nun Neotektonik Dönemde Jeolojik ve Yapısal Evrimi:
854 PhD Thesis, İstanbul Üniversitesi, Fen Bilimleri Enstitüsü,İstanbul, 240 pp.+7 foldouts

855 Seeber, L., Cormier, M.-H., McHugh, C., Emre, O., Polonia, A., Sorlien, C., 2006, Rapid
856 subsidence and sedimentation from oblique slip near a bend on the North Anatolian
857 transform fault in the Marmara Sea, Turkey: Geology, v. 34, pp. 933–936.

858 Şengör, A. M. C., 1979, The North Anatolian transform fault: its age, offset and tectonic
859 significance, Journal of the Geological Society of London, 136, pp. 269-282.

860 Şengör, A. M. C., 2011, İstanbul Boğazı niçin Boğaziçi'nde açılmıştır: in Ekinci, D.,
861 editor, Fiziki Coğrafya Araştırmaları: sistematik ve Bölgesel (Hoşgören volume), Türk
862 Coğrafya Kurumu Yayınları, no. 6, pp. 57-102

863 Şengör A. M. C, Görür N. and Şaroğlu, F., 1985, Strike-slip faulting and related basin
864 formation in zones of tectonic escape: Turkey as a case study: in Biddle K.T. and
865 Christie-Blick, N., editors, Strike-slip Deformation, Basin Formation, and Sedimentation,
866 Society of Economic Paleontologists and Mineralogists Special Publication 37 (in honor
867 of J.C. Crowell), pp. 227–64

868 Şengör, A. M. C. and Kidd, W. S. F., 1979, The post-collisional tectonics of the Turkish-

869 Iranian Plateau and a comparison with Tibet: Tectonophysics, v. 55, p. 361-376.

870 Şengör, A. M. C., and Natal'in, B.A., 1996, Palaeotectonics of Asia: Fragments of a
871 synthesis: in Tectonic Evolution of Asia, Rubey Colloquium, pp. 486-640, Eds. Yin, A.
872 and Harrison, M., Cambridge University Press, Cambridge.

873 Şengör, A. M. C., Özeren, S., Genç, T. and Zor, E., 2003, East Anatolian high plateau as a
874 mantle-supported, north-south shortened domal structure: Geophysical Research
875 Letters, v. 30, DOI: 10.1029/2003GL017858

876 Şengör, A. M. C., Özeren, M. S., Keskin, M., Sakınç, M., Özbakır, A. D., Kayan, I., 2008,
877 Eastern Turkish high plateau as a small Turkic-type orogen: implications for post-
878 collisional crust-forming processes in Turkic-type orogens. Earth Science Reviews, v. 90
879 pp. 1–48.

880 Şengör, A. M. C., Tüysüz, O., İmren, C., Sakınç, M., Eyidoğan, H., Görür, N., Le Pichon,
881 X., and Rangin, C., 2005, The North Anatolian Fault: A new look: Annual Review of
882 Earth and Planetary Sciences, 33, 37-112.

883 Şengör, A. M. C., Uçarkuş, G., İmren, C., Rangin, C., Le Pichon, X., Özeren, S., Natal'in,
884 B., 2011, Broad shear zones and narrow strike-slip faults in orogens and their role in
885 forming the orogenic architecture: The North Anatolian Fault as an active example,
886 Joint Meeting GeoMunich, Fragile Earth: Geological Processes from Global to Local

887 Scales, associated Hazards and Resources, 14-2, A18, Munich, Germany, September 4-7.

888 Şentürk, K. and Okay, A.I., 1984, Blueschists discovered east of Saros Bay in Thrace:
889 Bulletin of the Mineral Research and Exploration Institute of Turkey, 97/98, 72-75.

890 Shillington, D. J., Seeber, L., Sorlien, C. C., Steckler, M. S., Kurt, H., Dondurur, D., Çifçi,
891 G., İmren, C., Cormier, M.-H., McHugh, C. M. G., Gürçay, S., Poyraz, D., Okay, S.,
892 Atgın, O. and Diebold, J. B., 2012, Evidence for widespread creep on the flanks of the
893 Sea of Marmara transform basin from marine geophysical data: Geology, v. 40, pp. 439-
894 442.

895 Sorlien, C. C., Akhun, S. D., Seeber, L., Steckler, M. S., Shillington, D. J., Kurt, H., Çifçi,
896 G., Timur Poyraz, D., Gurcay, S., Dondurur, D., İmren, C., Perincek, E., Okay, S., Küçük,
897 H. M. and Diebold, J. B., 2012, Uniform basin growth over the last 500ka, North
898 Anatolian Fault, Marmara Sea, Turkey, Tectonophysics, v. 518-521, pp. 1-16.

899 Taymaz, T., Jackson, J. A., and McKenzie, D., 1991, Active tectonics of the north and
900 central Aegean Sea: Geophysical Journal International, 106, pp. 433-490.

901 Tchalenko, J. S., 1970, Similarities between shear zones of different magnitudes:
902 Geological Society of America Bulletin, 81, pp. 1625-1640.

903 Uçarkuş, G., 2010, Active faulting and earthquake scarps along the North Anatolian
904 fault in the Sea of Marmara: PhD. Thesis, İstanbul Technical University, Eurasia

905 Institute of Earth Sciences, xxx+178 pages.

906 Wilcox, R. E., Harding, T. P., and Seely, D. R., 1973, Basic wrench tectonics: The
907 American Association Petroleum Geologists Bulletin, 57/1, 74-96.

908 Wilson, J. T, 1965, A new class of faults and their bearing on continental drift: Nature,
909 207, 4995, 343–347.

910 Zitter, T. A. C., Grall, C., Henry, P. Özeren, S., Çağatay, M. N., Şengör, A. M. C.,
911 Gasperini, L., Mercier de Lépinay, B., Géli, L., 2012, Distribution, morphology and
912 triggers of submarine mass wasting in the Sea of Marmara: Marine Geology, v. 329-331,
913 pp. 58-74.

914

915 FIGURE CAPTIONS

916 Fig. 1. Wilson's illustration of the kinds of transform faults (Wilson, 1965, fig. 3). For
917 'arc' read 'trench' to conform to present common usage: A) a. ridge-ridge, b. ridge-arc
918 facing away from the ridge, c. ridge-arc facing toward the ridge (this is, in principle,
919 what the North Anatolian Fault is), d. arc-arc with arcs facing away from one another, e.
920 arc-arc with arcs facing the same way, f. arc-arc with arcs facing toward each other, B)
921 d. transform point at which extension changes to shortening.

922 Fig. 2. The North Anatolian Fault, forming in reality a family of faults that constitute the

North Anatolian Keirogen (Şengör et al., 2005). Not all the faults shown on this map are now active, but all have been active sometime in the last 11 Ma. Most are potential earthquake generators. Fault traces delineated by heavier lines represent the most active parts of the keirogen constituting the strands collectively known as the North Anatolian Fault (NAF). Note that the keirogen is entirely confined to the area underlain by Tethyside accretionary complexes shown in gray (Slightly modified from Şengör et al. (2005, Fig. 2)).

Fig. 3. The North Anatolian Shear Zone (NASZ: delimited by discontinuous lines) and the courses of the major rivers traversing it. Key to abbreviations: from east to west (Black letters): E=Elmalı/Peri (tributary of the Murat before the construction of the Keban Dam), Ka=Karasu (Elmalı/Peri+Karasu=Fırat {Euphrates} without Murat {outside this map}, Y=Yeşilırmak, K=Kızılırmak, D=Delice, F=Filyos (/Yenice/Araç/Soğanlı {formerly Uluçay}/Gerede Suyu), S=Sakarya, Su=Susurluk. Grey letters in outline show locations of some cities and tectonic features: A=Ankara, B=Bursa, b=Bolu, E=Erzincan, İ=İstanbul, İ=İznik (lake) K=Karlıova, OF=Ovacık Fault, SF=Sungurlu Fault. Notice that significant abrupt deflections of river courses are confined to the area of the NASZ. Following Şengör et al. (2005), the faults shown to be parts of the NASZ in the southern part of the Tokat Lobe are here left out of the NASZ because of their as yet uncertain relationship to the NASZ and to the geometry of the major river courses (Slightly modified from Şengör et al. (2005, Fig. 6)).

943 Fig. 4. Historical earthquake epicentres in and around the Sea of Marmara compiled by
944 the ETH Geodesy and Geodynamics Laboratory (GGL), Zurich. Most of these
945 earthquakes presumably occurred on the faults shown in Fig. 5.

946 Fig. 5. A. The locations of the multichannel seismic profiles used in this study.
947 CB=Central basin, CiB= Cinarcik Basin, ET=Erdek Tombolo, GG= Gulf of Gemlik,
948 KB=Kumburgaz Basin, MI=Marmara Island, TB=Tekirdağ Basin. B. The faults mapped
949 in this study. The black segments are active and the grey segments are presumably
950 inactive.

951 Fig. 6. Maps of the eastern sector of our study area: A. Location map of the profiles
952 selected to characterise the faults in this sector. B. Distribution of seismicity during the
953 2005-2011 interval in the eastern sector. C. Distribution of seismicity compared with the
954 identified faults belonging to the North Anatolian Shear Zone. Refer to the Fig. 5 for the
955 legend of the faults.

956 Fig. 7A. Line 9 showing a cross section across the Çınarcık Basin including its broad
957 southern shelf that contains a subsidiary basin on a southerly-tilted normal fault block.
958 B. Our interpretation of the structure of the Çınarcık Basin along Line 9 (vertical
959 exaggeration here is 4 times). In this profile, three onlap surfaces (pinch-outs , indicated
960 by black arrows) are observed at both basin edges as well as on the 2-km-wide faulted
961 anticline rising within the basin. These pinch-outs are thus most likely related to
962 variations in sedimentation rates rather than to changes in fault activity. The onlap

surfaces are assigned to the Red, the Blue and the Yellow sequences boundaries (130, 250 and 330 ka respectively). The thickness of 100 ka stratigraphic sequences in this case ranges between 400 ms twt and 150 ms twt (corresponding roughlty to 300 m and 110 m), which is consistent the mean sedimentation rates in this area (Seeber et al., 2006); as well as the sequences jump correlated by Sorlien et al., (2012, fig. 8). C. Same as Fig. 8B, but with no vertical exaggeration to show the 'real' geological structure. We have done this only for this profile to give an idea about the difference between the vertically exaggerted and non-exaggerated sections for those not used to looking at seismic profiles.

Fig. 8A. Line 13 showing another cross section farther west than line 9 across the Çınarcık basin showing a subbasin. B. Our interpretation of the structure of the Çınarcık Basin along Line 13 (vertical exaggeration here is 4 times) the sequences appear less obvious (exception for the pinch-out on the Red Horizon) but horizons have been correlated to the line 9, and this correlation looks in agreement with the interpretation of Sorlien et al. (2012, fig. 8). To the south, across the Imrali Basin, a thick coherent section of sedimentary horizons (reaching more than 3 s twt) is imaged. As in the Çınarcık Basin, pinch-outs can be recognized but the most remarkable feature is probably the toplap geometry (indicated by white arrow) at the base of the Blue (250 ka) horizon (also drawn on the fig. 4 in Sorlien et al., 2012). We assigned the same sequence boundary as Sorlien et al. (2012) in this area, and we note that onlap geometry on the

sequences boundaries, are also observed in this basin.

Fig. 9. Development of a shear zone (from Şengör, in press). Brown areas are structures associated with extension and/or transtension. In transtension, all extensional structures become 'flatter' and all shortening structures become 'steeper' with respect to the Y-shear. However, this is only an instantaneous picture, because as the shear zone evolves, all structures will rotate and strains will increase as we now see in the Sea of Marmara case. Key to lettering: F is fold axial trace, P is P-shear, R is a Riedel shear, R' is an anti-Riedel shear, T is a tension gash (in meso and macro examples, depending on the complexity of the stystem, the stress along the 'tension gash orientation' line may not necessarily be purely tensional, but there must be a major component of extension), X is an X shear. φ is the angle of internal friction of the material being sheared.

Fig. 10. Maps of the central sector of our study area: A. Location map of the profiles selected to characterise the faults in this sector. B. Distribution of seismicity during the 2005-2011 interval in the central sector. C. Distribution of seismicity compared with the identified faults belonging to the North Anatolian Shear Zone.

Fig. 11A. Line 23 showing a cross-section across the eastern moiety of the Kumburgaz Basin showing the well-localised basin and its temporal enlargement outward. For details of the seismic stratigraphy, see the caption of Fig. 10B. B. Our interpretation of the geology along line 23.

1002 Fig. 12A. Line 27 showing another cross section farther west than line 23 across the
1003 western moiety of the Kumburgaz Basin showing a broad, very young, bovine-head
1004 basin that is nested on the older, narrower, fault-bounded basin. B. Our interpretation
1005 of the geology along line 27. On both profiles, 23 and 27 pinch-outs of horizons on the
1006 Red (130 ka) and the Blue (250 ka), as well as on the Violet (430 ka) horizons are
1007 indicated by black arrows. The depth of these horizons along the Northern Main Fault
1008 are similar to the one proposed by Sorlien et al., 2012 (figs. 6 and 11), and implies a
1009 mean sedimentation rate of around 1-1.5 mm/a over 100 ka period. The well-localised
1010 basin below the blue Horizon, which was widened slowly outward through time, The
1011 blue sequence (250 ka) time, by contrast, looks like the period when the basin widening
1012 set on drastically. This change is concomitant to the deactivation/slowdown of the
1013 faults running across the Kumburgaz Basin. Part of these faults are presumably still
1014 active as some en-échelon discrete structures can be recognized along them on the
1015 seafloor (en-échelon structures mentioned in Fig. 11).

1016 Fig. 13. Maps of the western sector of our study area: A. Location map of the profiles
1017 selected to characterise the faults in this sector. B. Distribution of seismicity during the
1018 2005-2011 interval in the western sector. C. Distribution of seismicity compared with the
1019 identified faults belonging to the North Anatolian Shear Zone.

1020 Fig. 14A. Line 70 showing a cross section across the Western High showing its faulted
1021 anticline structure and the saucer-shaped basin in which the anticline seems to have

risen along its bounding faults. B. Our interpretation of the geology along line 70. This basin displays a thick coherent sedimentary section (which can reach 2 s twt of thickness), suggesting a long history of sedimentation. Along the basin margins one sees the very same seismic facies as one does within the lall perched basins on top of the High (to be published in Grall et al., in press, b). In particular one recognises the chaotic reflectors intrepreted as slide deposits on the violet horizon (430 ka) and also the bed with low amplitude reflectors above the green horizon (which is widespread in the entire Sea of Marmara). These observations show that the Western High rose in a basin that was simply an eastern continuation of the Tekirdağ Basin! The blue patchy reflector (250 ka) and the Red horizon in reverse polarity (130 ka) have been also recognized above these characteristic layers. This profile confirms what Grall et al. (in press a) pointed out regarding the Mass Transport Deposits on the Violet Horizon which is likely related to a regional (at least at the scale of the Western High) process (such as the paleo-environmental changes proposed in Grall et al., in press a).

Fig. 15A. Line 78 showing another cross section farther west than line 70 across the Tekirdağ Basin showing the central anticline covered with young sedimentary layers. B. Our interpretation of the geology along line 78. Note the fault that bounds the anticline to the north. It now seems vertical, but the internal structure of the anticline implies that it might have originated as a very-steeply south-dipping thrust fault, contrary to the interpretation by Okay et at. (1999). 1.5 s of coherent sedimentary section is imaged

1042 across the Tekirdağ Basin, on which onlap sequences (indicated by black arrows) occur
1043 periodically, as in the Central Basin (Grall et al., 2012), and in the Çınarcık (Fig. 8A). The
1044 first Red onlap surface (dated at ~130 ka) is at around 300 ms twt (roughly 230 m)
1045 below the seafloor within the depocentre. This age estimation is thus consistent with the
1046 mean sedimentation rates (1.5-2mm/a) derived from the last marine/lacustrine
1047 transition (Mercier de Lepinay, pers. comm). The transparent lens in green (430-540 ka
1048 interval) in the basin as well as in the bounded anticline, looks very similar to the one
1049 encountered on the Western High and elsewhere in the Sea of Marmara (Grall et al., in
1050 press b). The Red and the Blue horizons have been correlated from the basin to the
1051 southern anticline across the faults. The Red Horizon is tentatively proposed on the
1052 base of sediments affected by gravitay-gliding, as it has been shown that main slides
1053 occur preferentially during glacial/interglacial transitions (Grall et al., in press a).
1054 Nonetheless, we cannot exclude that the prominent reflector on the base of this sliding
1055 mass, which apparently functions as a *décollement* could have no stratigraphic meaning.
1056 Besides, it is also probably interesting to note that across this basin as across other deep
1057 basins, no mass transports deposits have yet been recognized on top of the violet
1058 horizon, despite the fact that they have been recognized in the ponded basins of the
1059 Western High (Grall et al., in press b), as well as on the margins of the basin within
1060 which the Western High seems to rise (Fig. 13B).

1061 Fig. 16. Profile 84 across the Mt. Ganos shelf and slope showing the underthrusting of

1062 the Tekirdağ Basin floor under the rising pillar of Mr. Ganos and the development of a
1063 small marginal fold-thrust belt. This underthrusting activity is probably the reason of
1064 the microseismicity seen along the small faults at high angles to the overthrust margin
1065 breaking up the basin floor (Fig. 12C).

1066 Fig. 17. The locations, magnitudes and the first-motion solutions of the major shocks
1067 known from the southern part of the western sector studied in this paper. Fault plane
1068 solutions are from McKenzie (1972), Ekström and England (1989), and Taymaz et al.
1069 (1991).

1070 Fig. 18A. A simplified map of the faults reported in this paper. The two light blue
1071 patches are the Central and the Western Highs. B. Same as A, but with a left-lateral
1072 shear imposed on all the elements to reverse the right-lateral shear of some 55 km along
1073 the Sea of Marmara. C. A comparison of the present geometry of the faults belonging to
1074 the northern part of the north Anatolian Shear Zone in the Sea of Marmara with their
1075 presumed geometry before a homogeneous right-lateral shear of some 55 km took
1076 place. Note how little many of the elements rotate. No wonder so many of the R shears
1077 are so long-lived. Note also that the Central and the Western Highs are compressed into
1078 a more pronounced NE-SW orientation as the shear evolves. The compression appears
1079 as a rotation of the entire structure, which, in reality, it is not.

1080 Fig. 19. The presumed geometry of the fault network depicted in Fig. 18A at a depth of
1081 about 10 km below the floor of the Sea of Marmara. All the faults are assumed to have

widened into shear zones with a uniform width of 4 km. This is probably wrong, as not all faults have the same displacement, but it gives an idea as to what the North Anatolian Fault family under the Sea of Marmara may look like close to mid-crustal depths. The inset marked 'b' is a hand specimen showing the mesostructure of the Ailao shear zone at amphibolite facies metamorphic conditions. Its similarity to our presumed North Anatolian fault structure at depth is remarkable.

FIGURES

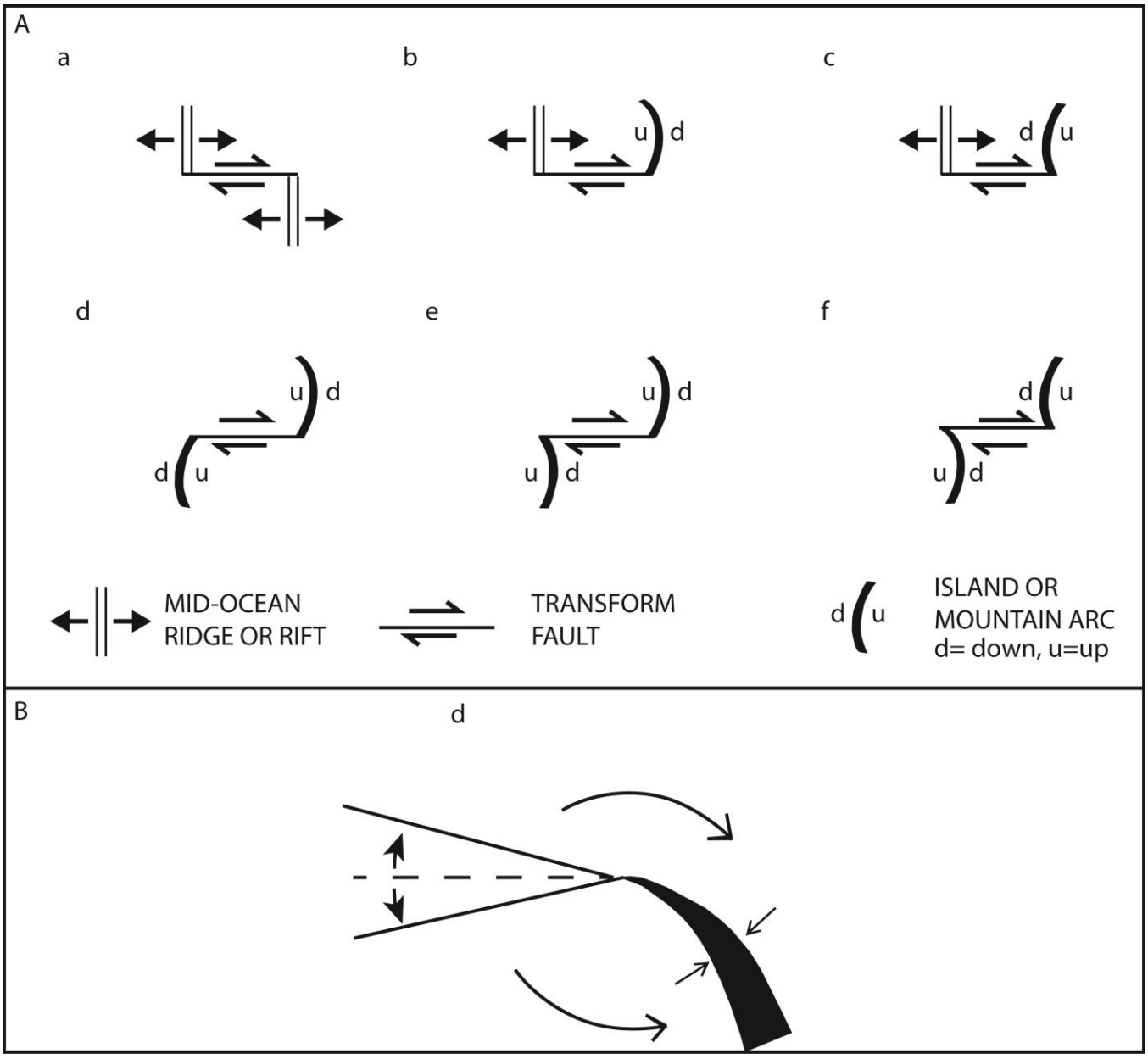
A
a
b
u
d
c
d
u
d
u
d
d
u
e
u
d
u
d
f
d
u
u
d
MID-OCEAN
RIDGE OR RIFT
TRANSFORM
FAULT
d
u
ISLAND OR
MOUNTAIN ARC
d= down, u=up
B
d

1090

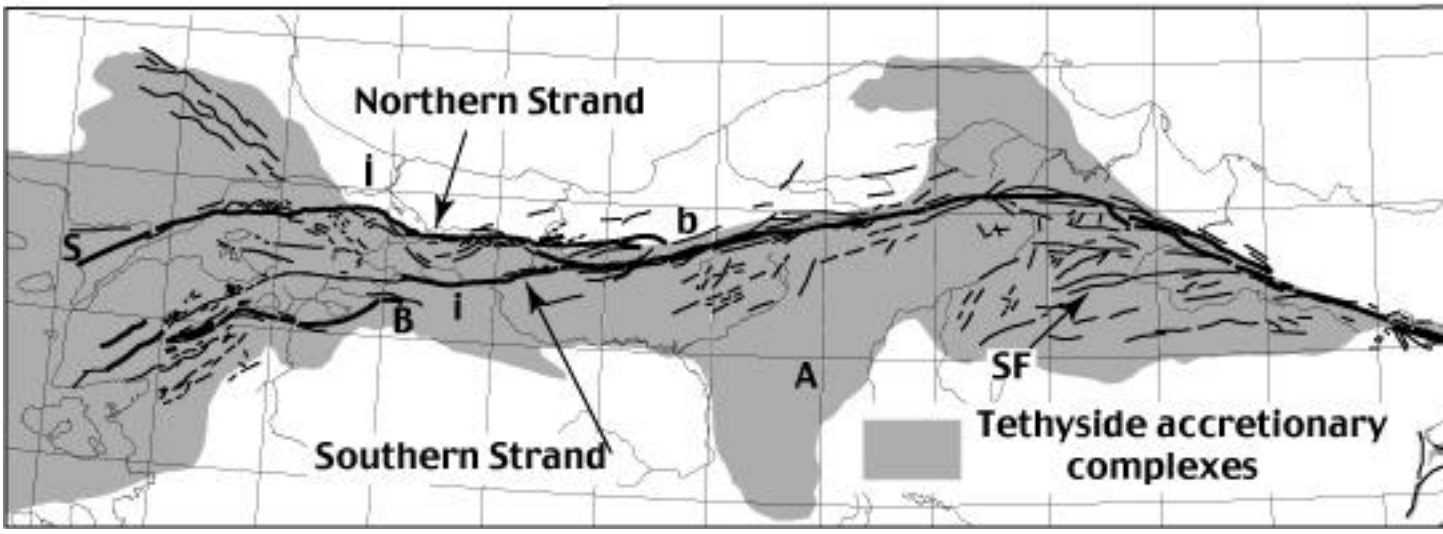
Northern Strand
i
b
S
B
i
A
SF
Southern Strand
Tethyside accretionary complexes

1091

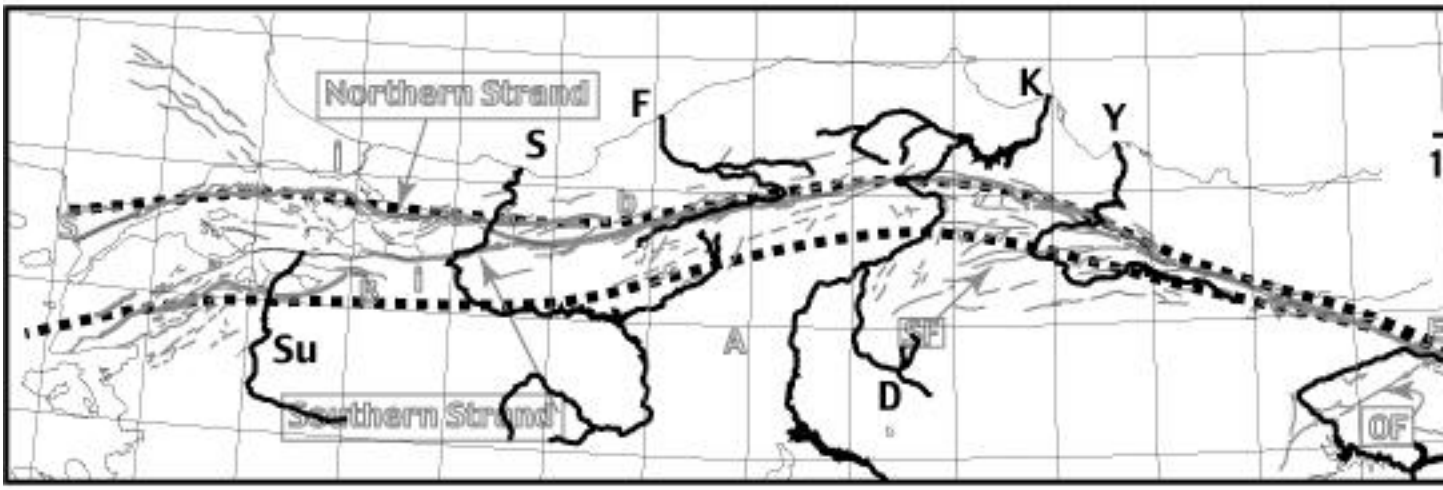
Northern Strand
F
K
Y
S
Su
A
D
OF

1092

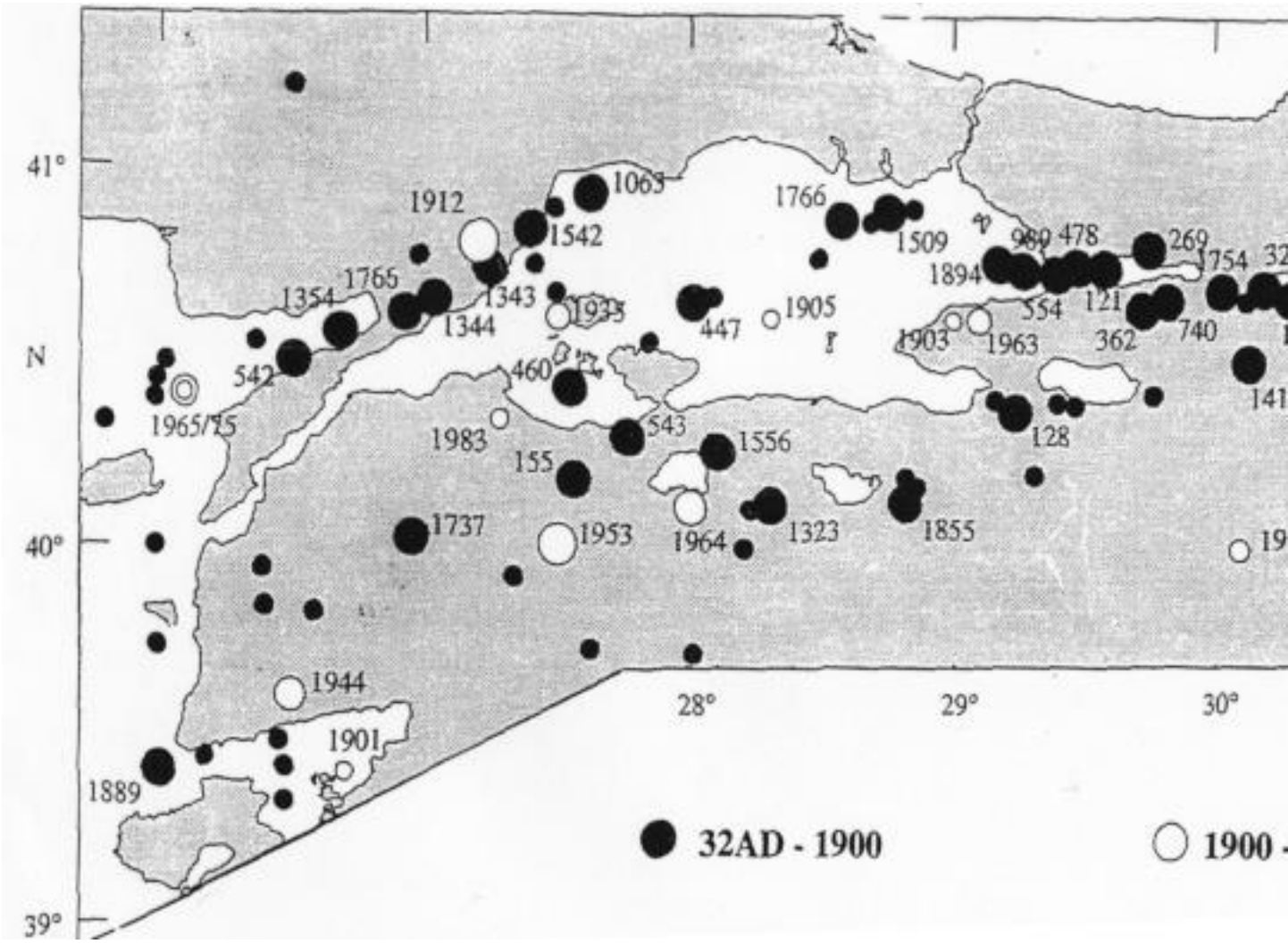
41°
N
40°
39°
28°
29°
30°
1912
1063
1542
1766
1509
989
478
269
1894
1754
1765
1354
1343
1344
1935
1905
447
554
121
740
362
1903
1963
542
460
1965/75
1983
543
1556
155
128
1737
1953
1964
1323
1855
1944
1901
1889
32AD - 1900
1900 -

1093

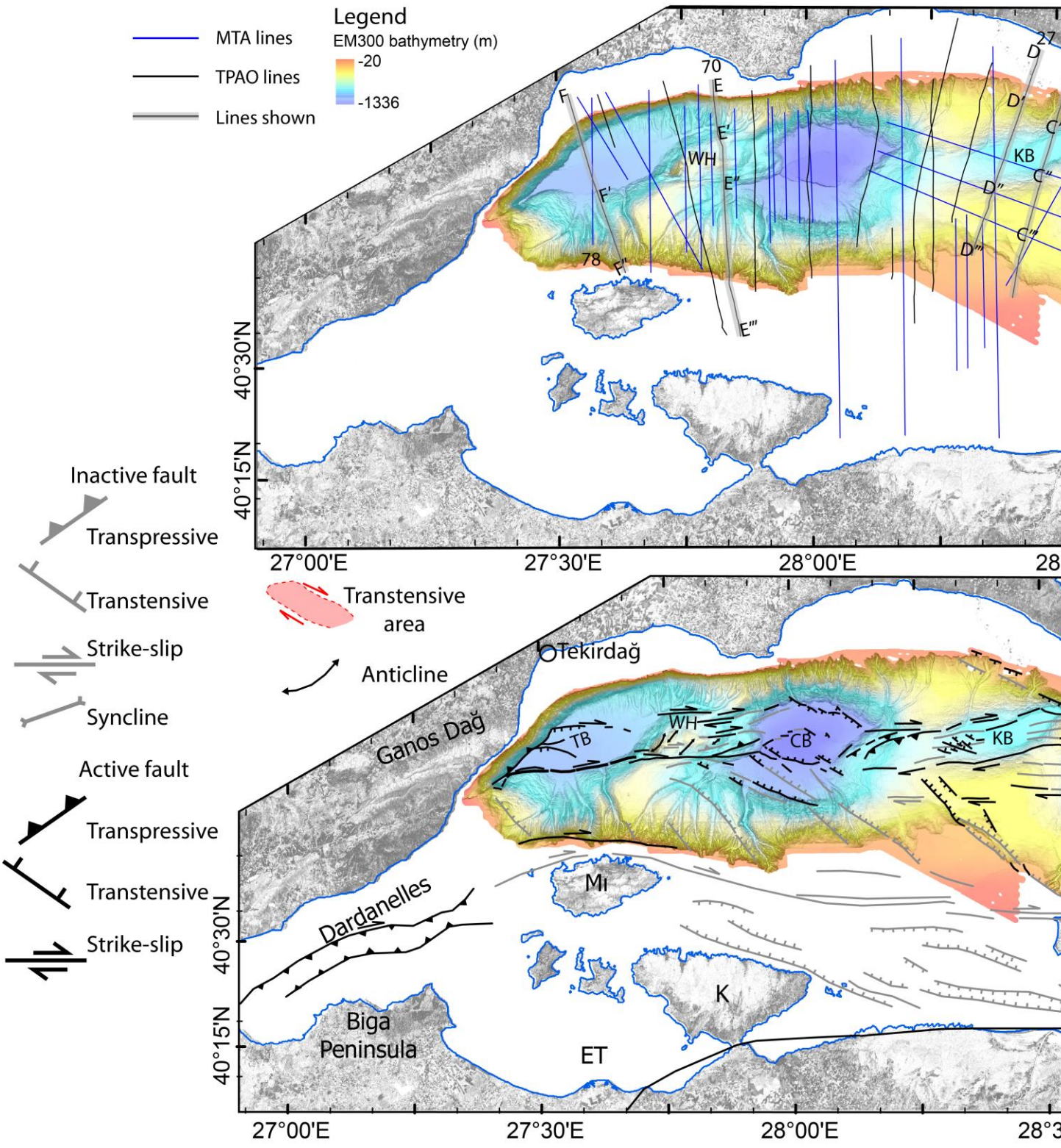
Legend
MTA lines
TPAO lines
Lines shown
EM300 bathymetry (m)
-20
-1336
70
78
27
E
E′
E″
E‴
F
F′
F″
WH
D
D′
D″
D‴
C′
C″
C‴
KB
40°30'N
40°15'N
27°00'E
27°30'E
28°00'E
Inactive fault
Transpressive
Transtensive
Strike-slip
Syncline
Transtensive area
Anticline
Active fault
Transpressive
Transtensive
Strike-slip
Tekirdağ
Ganos Dağ
TB
WH
CB
KB
Dardanelles
MI
K
Biga Peninsula
ET

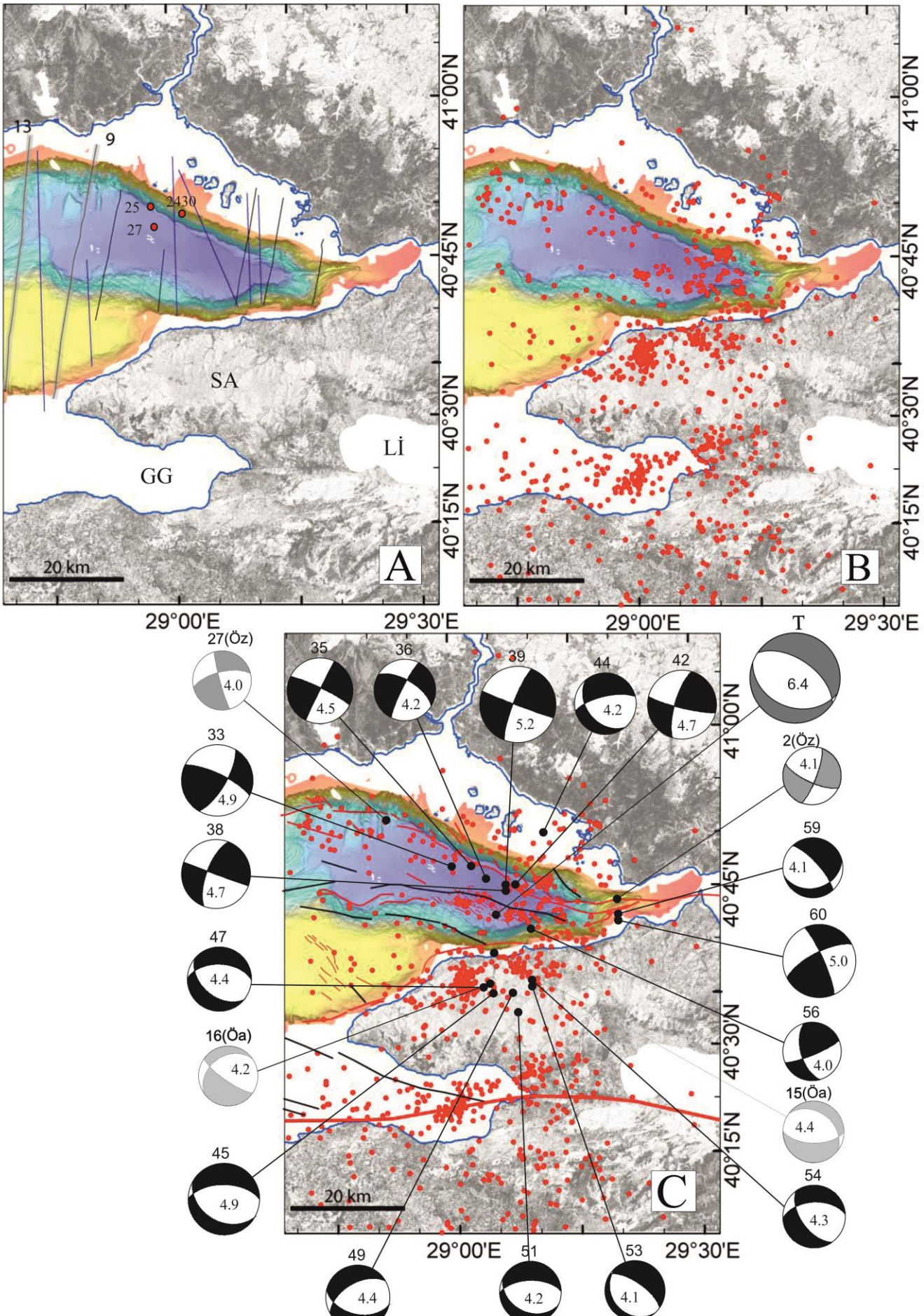
13
9
25
2430
27
SA
Lİ
GG
20 km
A
B
C
41°00'N
40°45'N
40°30'N
40°15'N
29°00'E
29°30'E
27(Öz)
4.0
35
4.5
36
4.2
39
5.2
44
4.2
42
4.7
T
6.4
33
4.9
2(Öz)
4.1
38
4.7
59
4.1
47
4.4
60
5.0
16(Öa)
4.2
56
4.0
15(Öa)
4.4
45
4.9
54
4.3
49
4.4
51
4.2
53
4.1

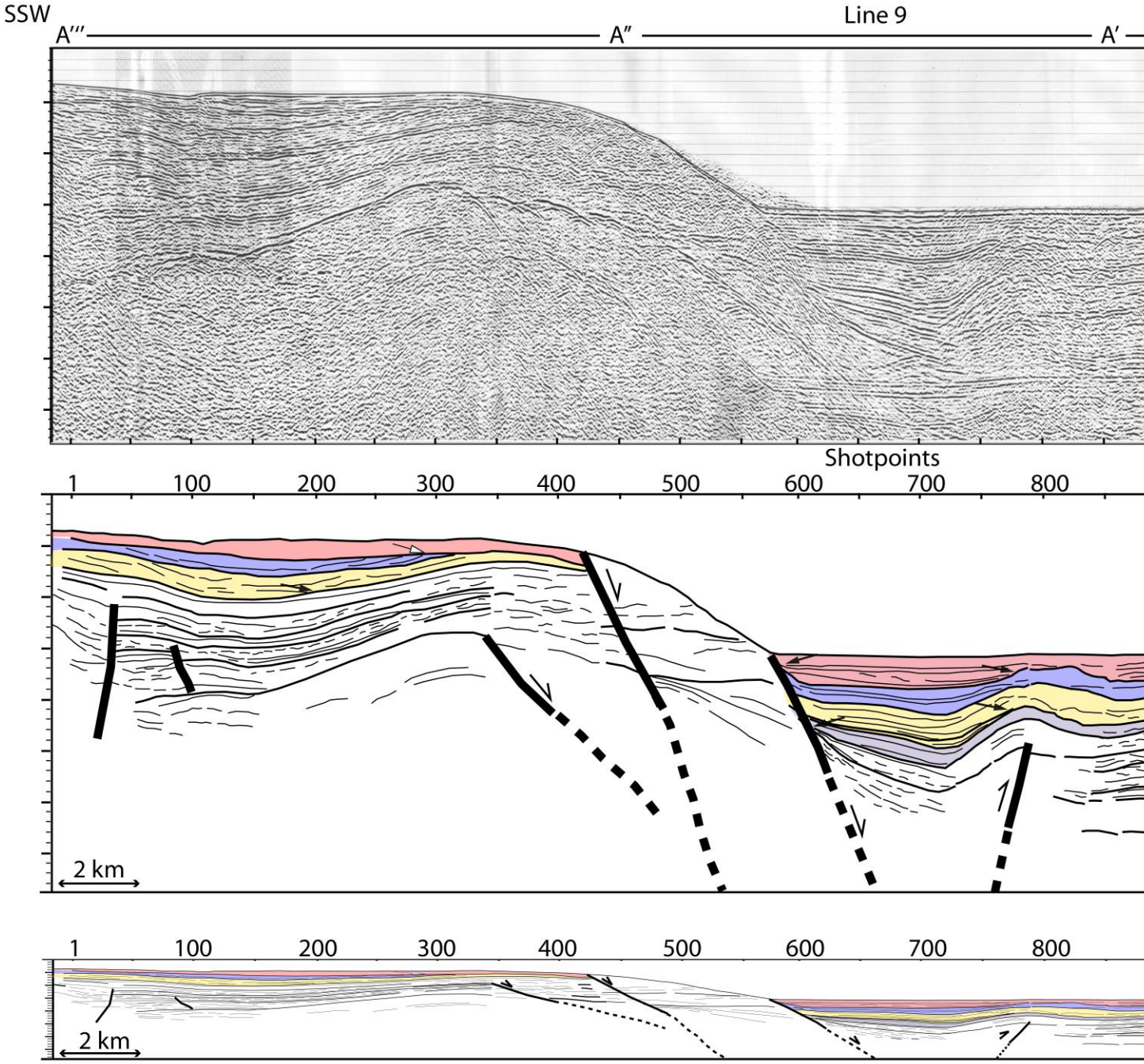
SSW
A‴
A″
Line 9
A′
Shotpoints
1
100
200
300
400
500
600
700
800
2 km
1
100
200
300
400
500
600
700
800
2 km

1096

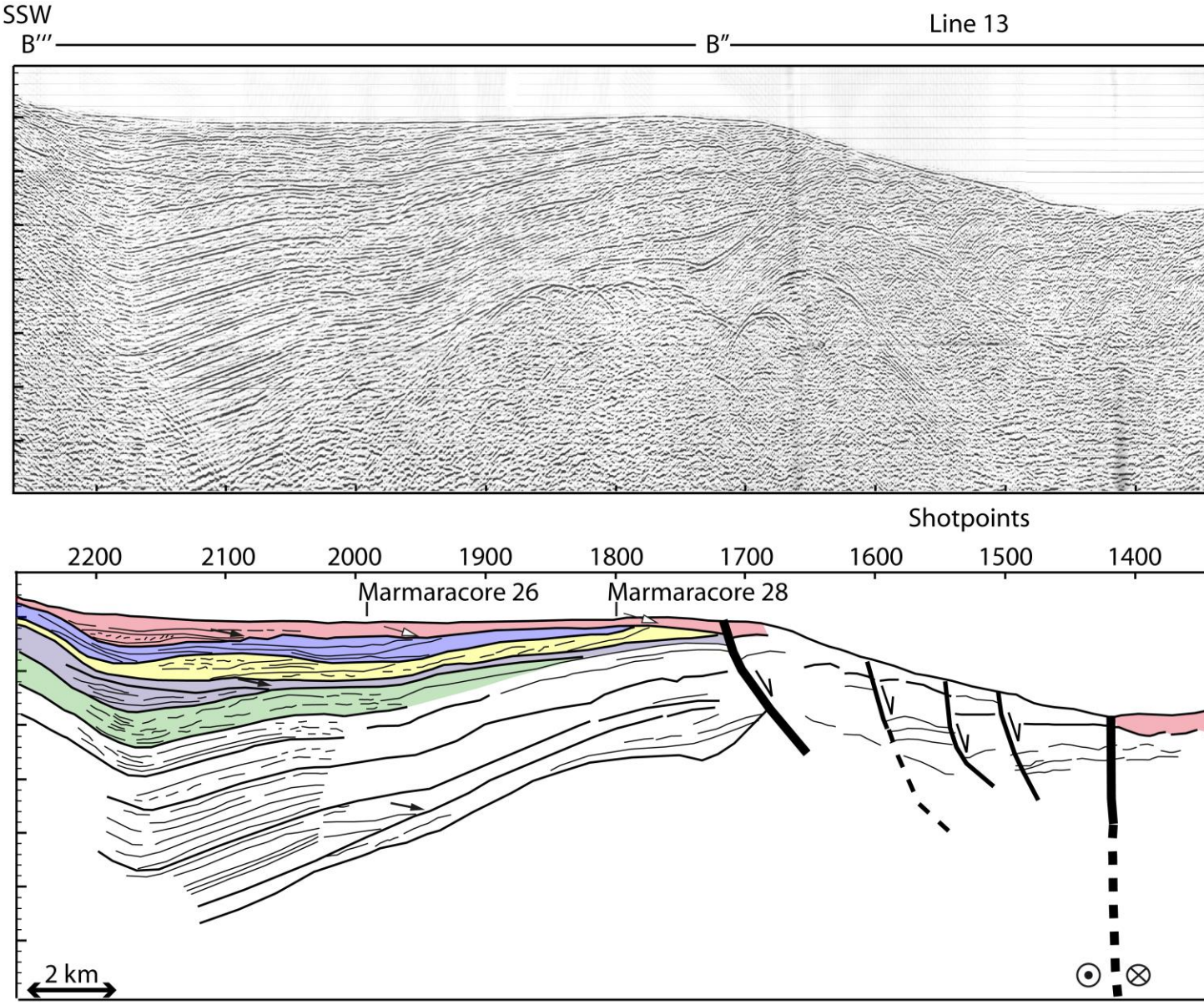
SSW
B‴
B″
Line 13
Shotpoints
2200
2100
2000
1900
1800
1700
1600
1500
1400
Marmaracore 26
Marmaracore 28
2 km

1097

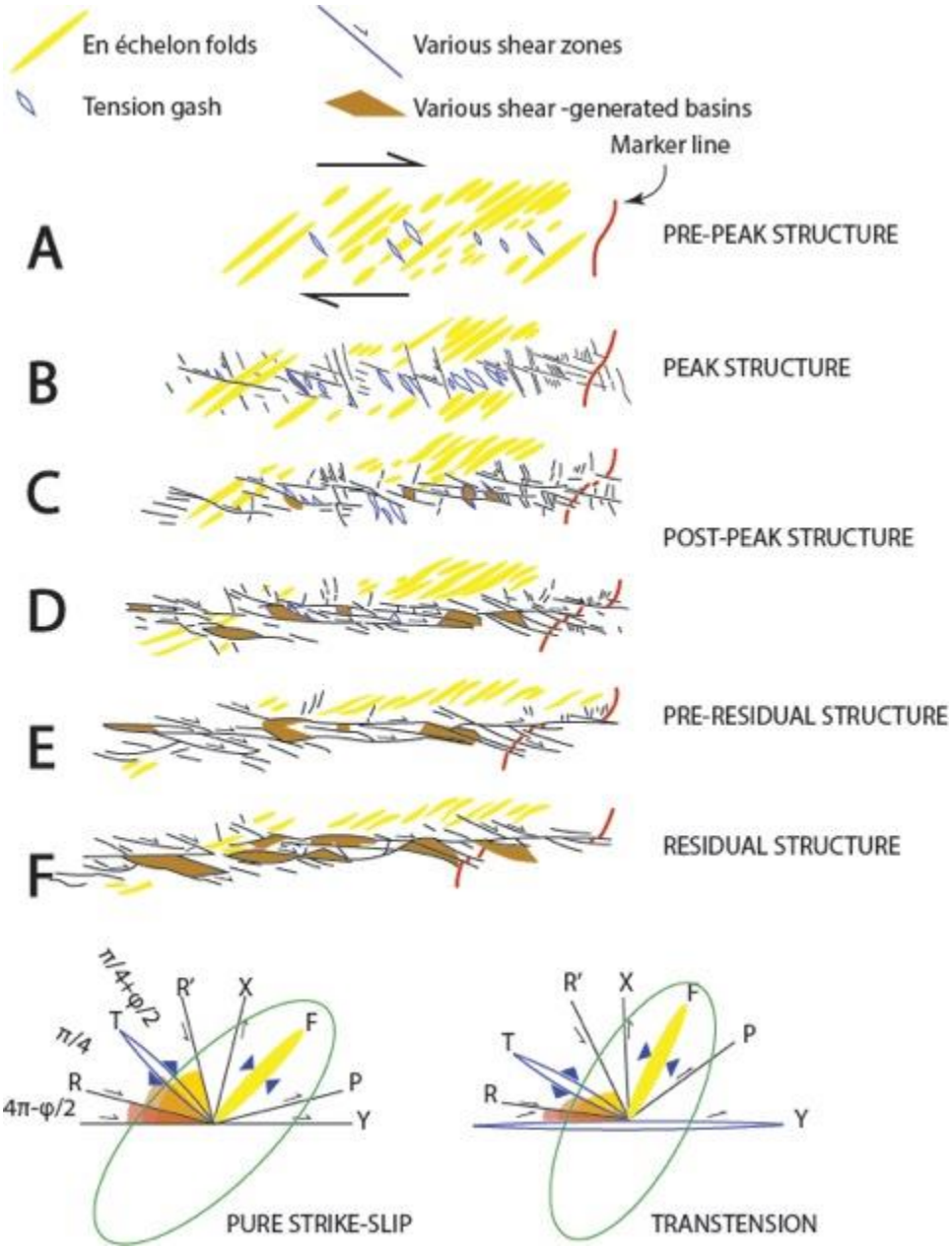
En échelon folds
Various shear zones
Tension gash
Various shear -generated basins
Marker line
A
PRE-PEAK STRUCTURE
B
PEAK STRUCTURE
C
POST-PEAK STRUCTURE
D
E
PRE-RESIDUAL STRUCTURE
F
RESIDUAL STRUCTURE
π/4+φ/2
R'
X
T
F
π/4
R
P
4π-φ/2
Y
PURE STRIKE-SLIP
R'
X
F
T
P
R
Y
TRANSTENSION

1098

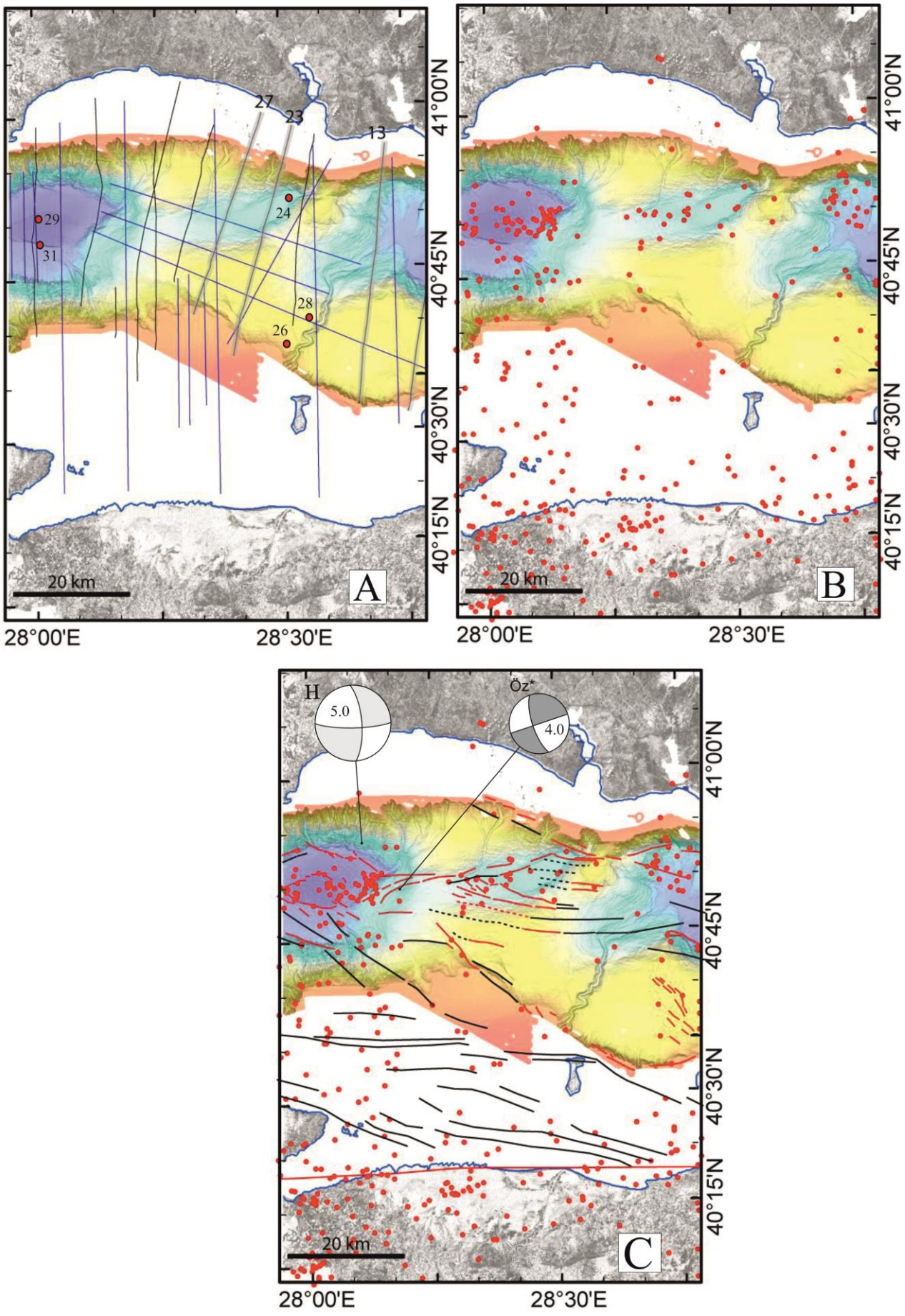
27
23
13
24
29
31
28
26
20 km
A
B
C
H
5.0
Öz*
4.0
41°00'N
40°45'N
40°30'N
40°15'N
28°00'E
28°30'E

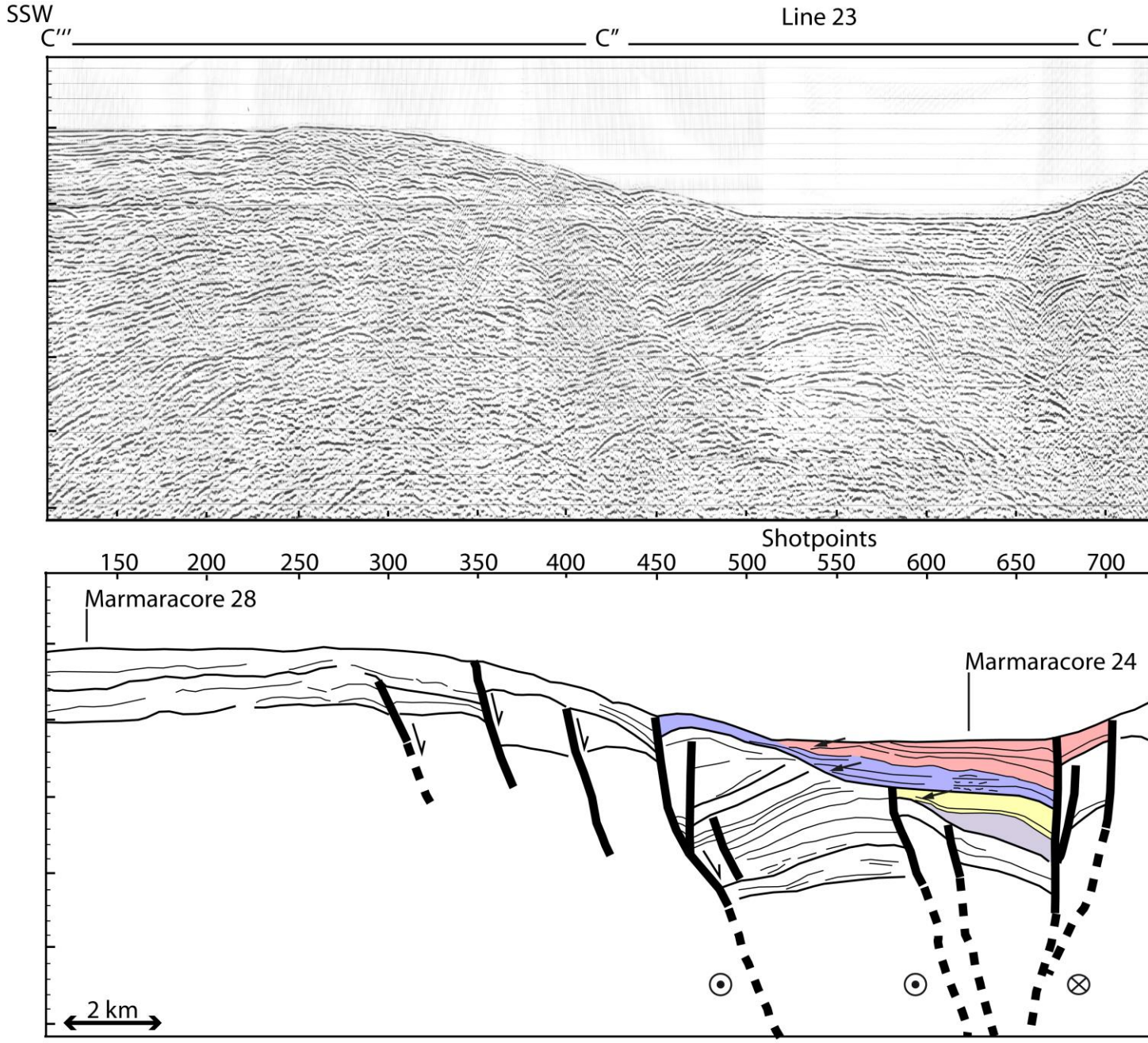
SSW
C‴
C″
Line 23
C′
Shotpoints
150
200
250
300
350
400
450
500
550
600
650
700
Marmaracore 28
Marmaracore 24
2 km

1100

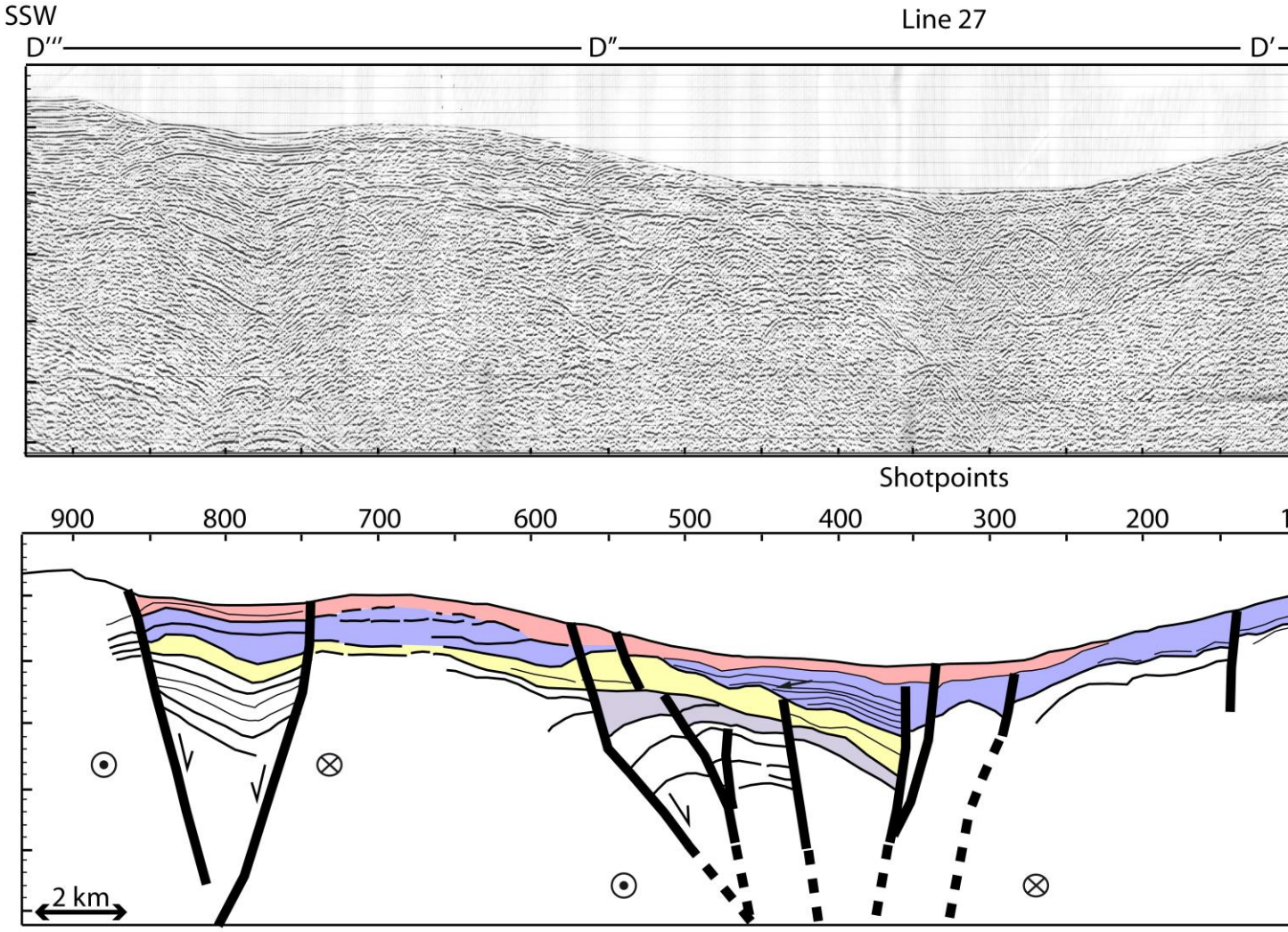

1101

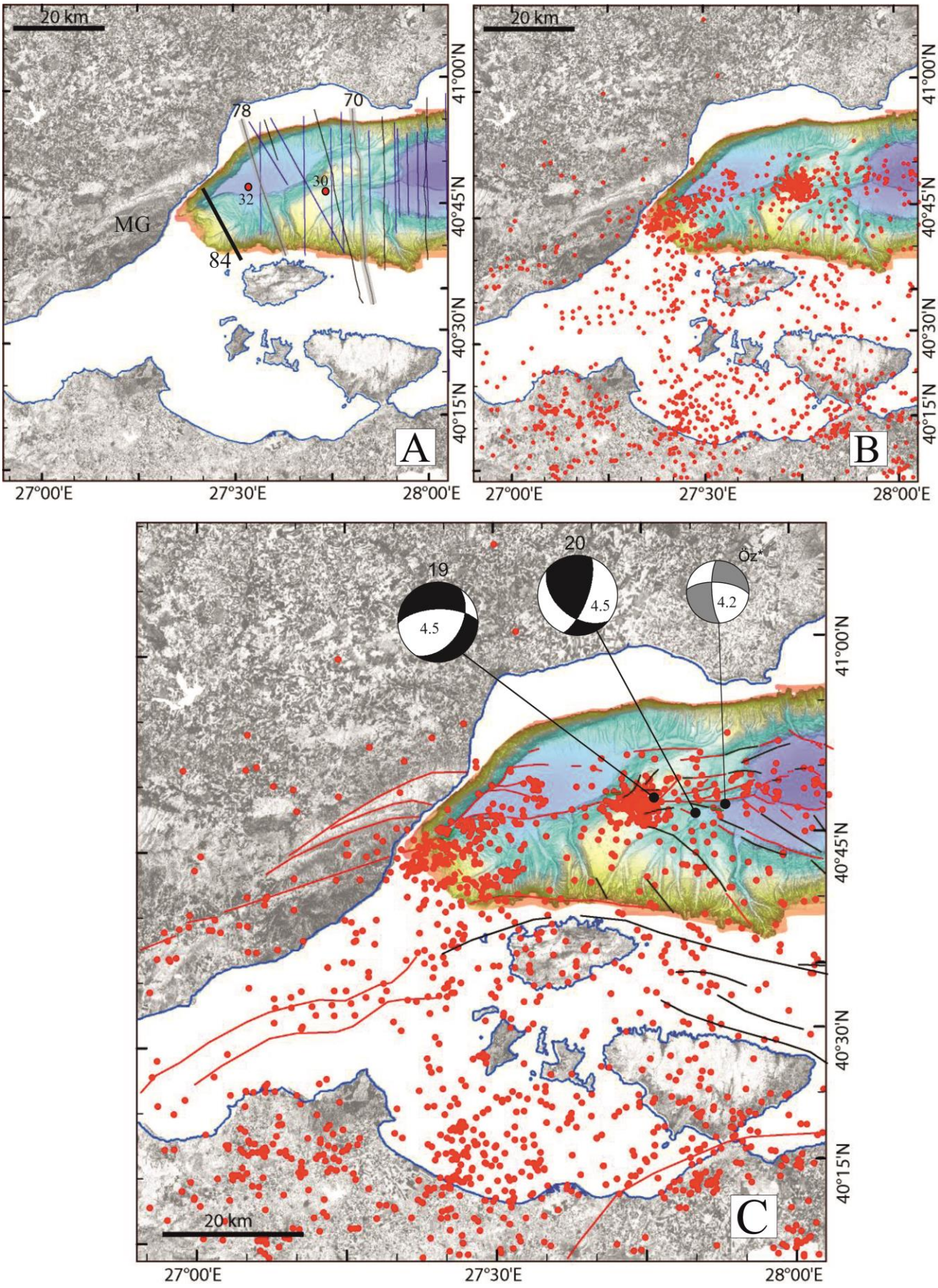
20 km
78
70
30
32
MG
84
A
41°00'N
40°45'N
40°30'N
40°15'N
27°00'E
27°30'E
28°00'E
20 km
B
19
4.5
20
4.5
Öz*
4.2
C
20 km

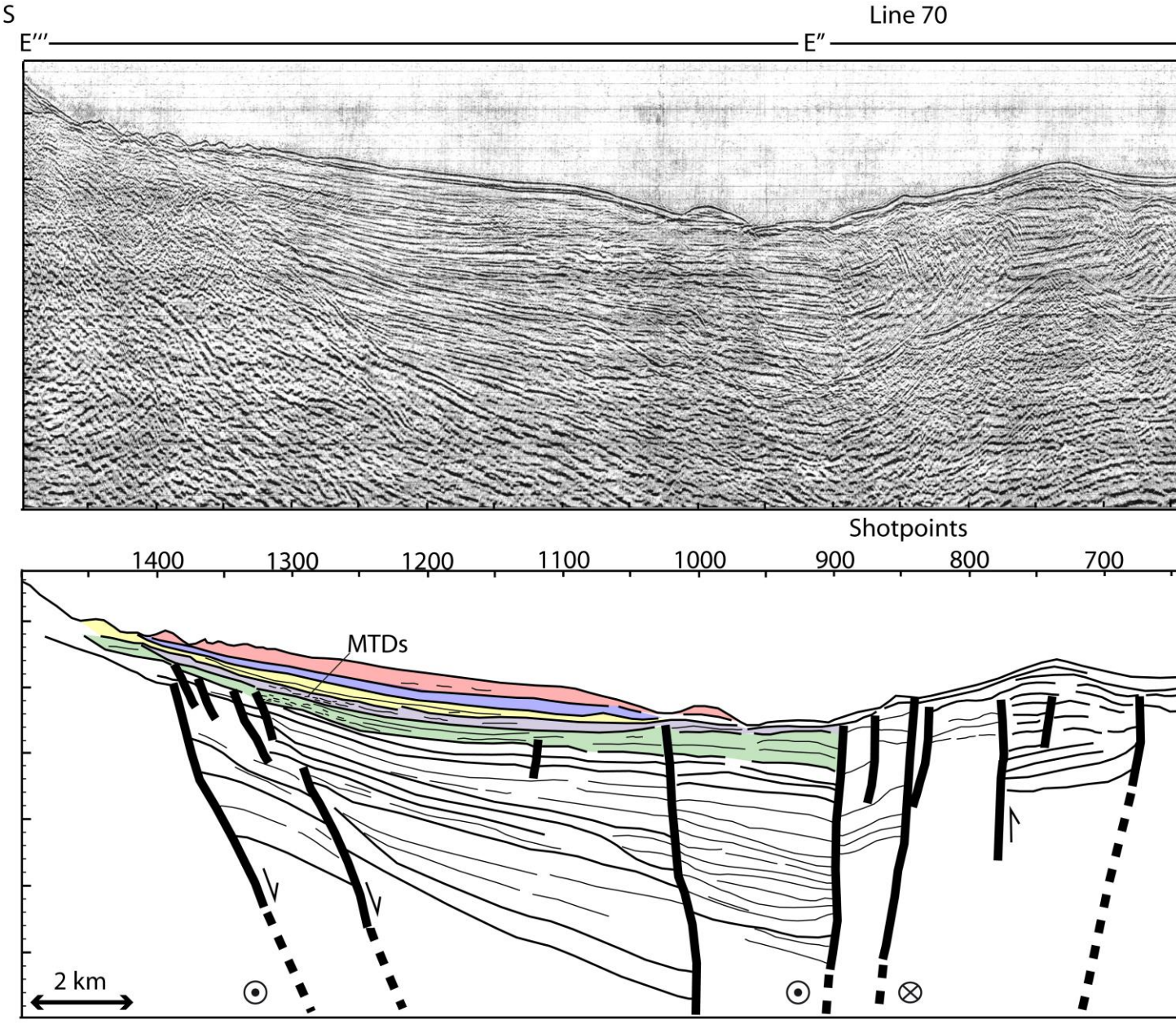
S
Line 70
E‴
E″
Shotpoints
1400
1300
1200
1100
1000
900
800
700
MTDs
2 km

1103

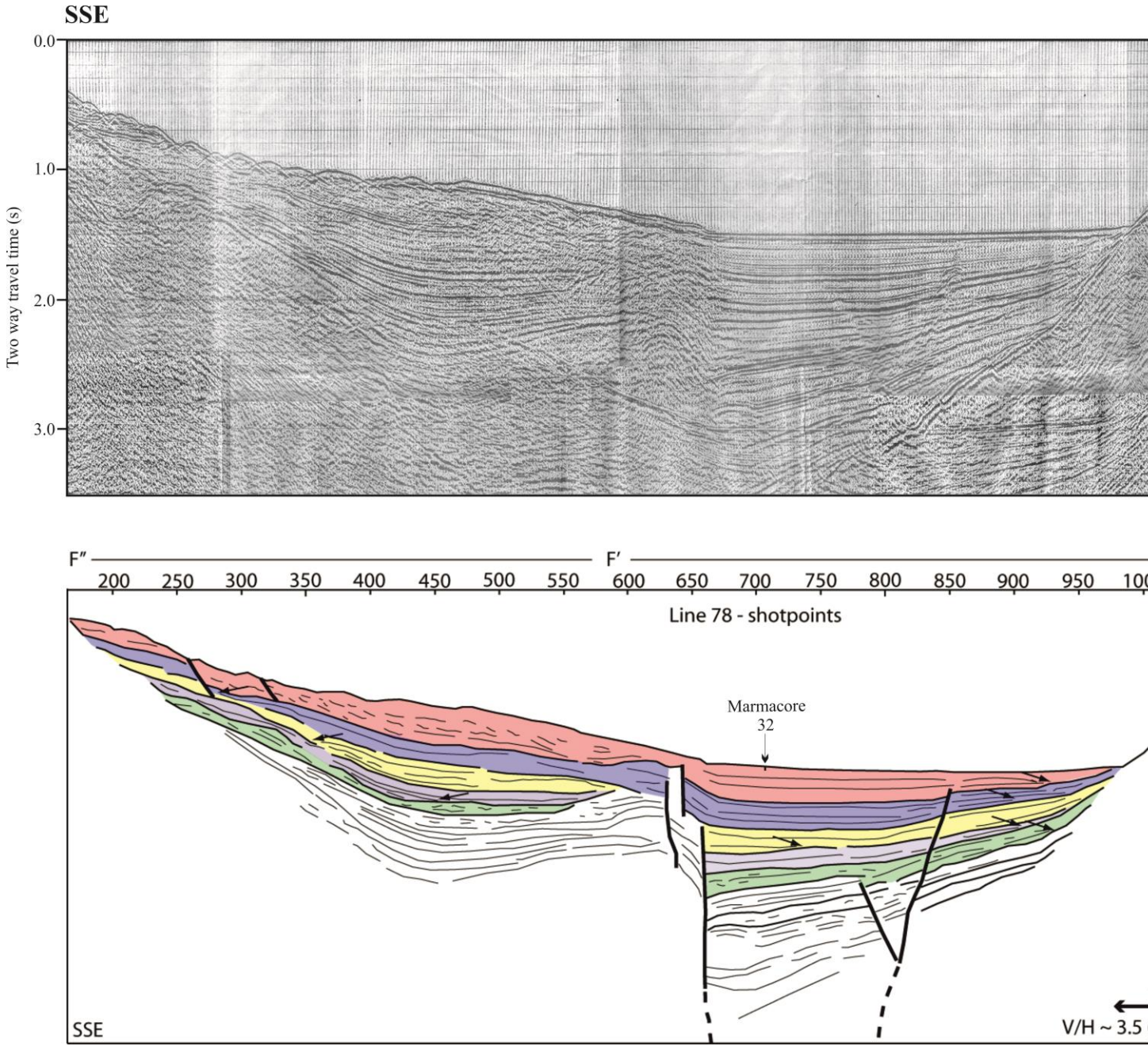
SSE
0.0
1.0
2.0
3.0
Two way travel time (s)
F″
F′
200
250
300
350
400
450
500
550
600
650
700
750
800
850
900
950
Line 78 - shotpoints
Marmacore
32
SSE
V/H ~ 3.5

1104

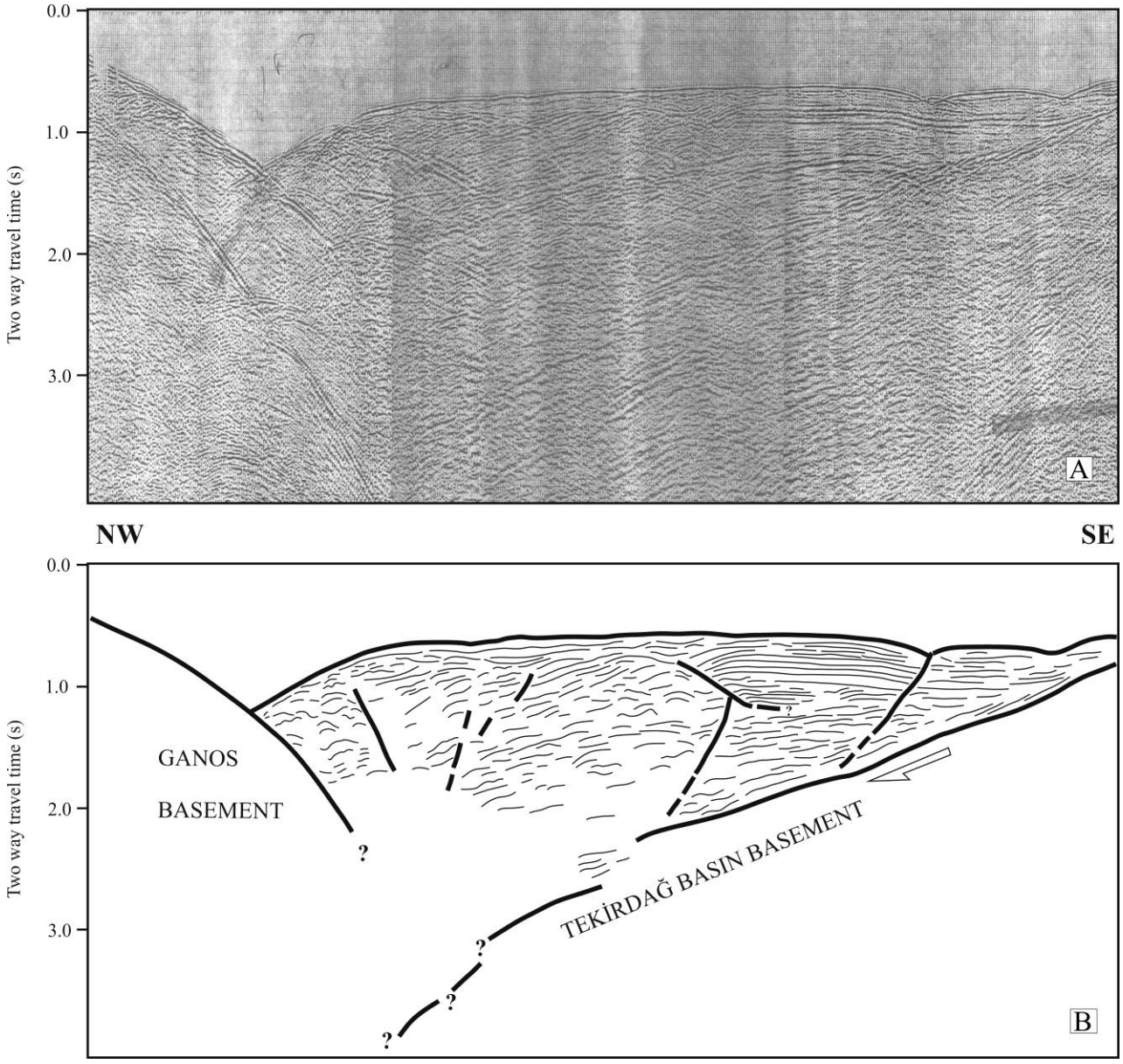
0.0
1.0
2.0
3.0
Two way travel time (s)
A
NW
SE
0.0
1.0
2.0
3.0
Two way travel time (s)
GANOS
BASEMENT
TEKİRDAĞ BASIN BASEMENT
?
?
?
?
B

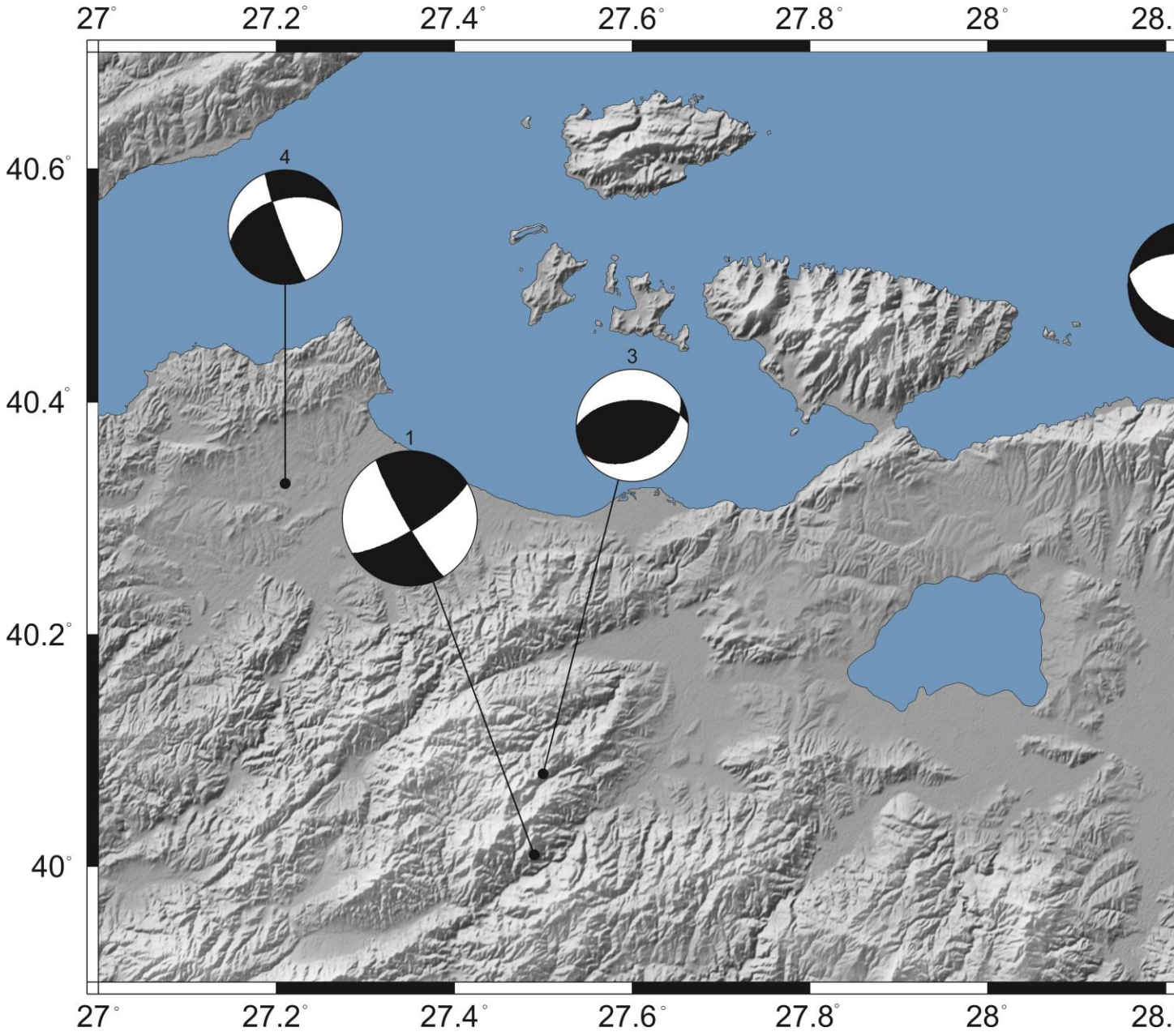
27°
27.2°
27.4°
27.6°
27.8°
28°
28.
40.6°
40.4°
40.2°
40°
4
3
1

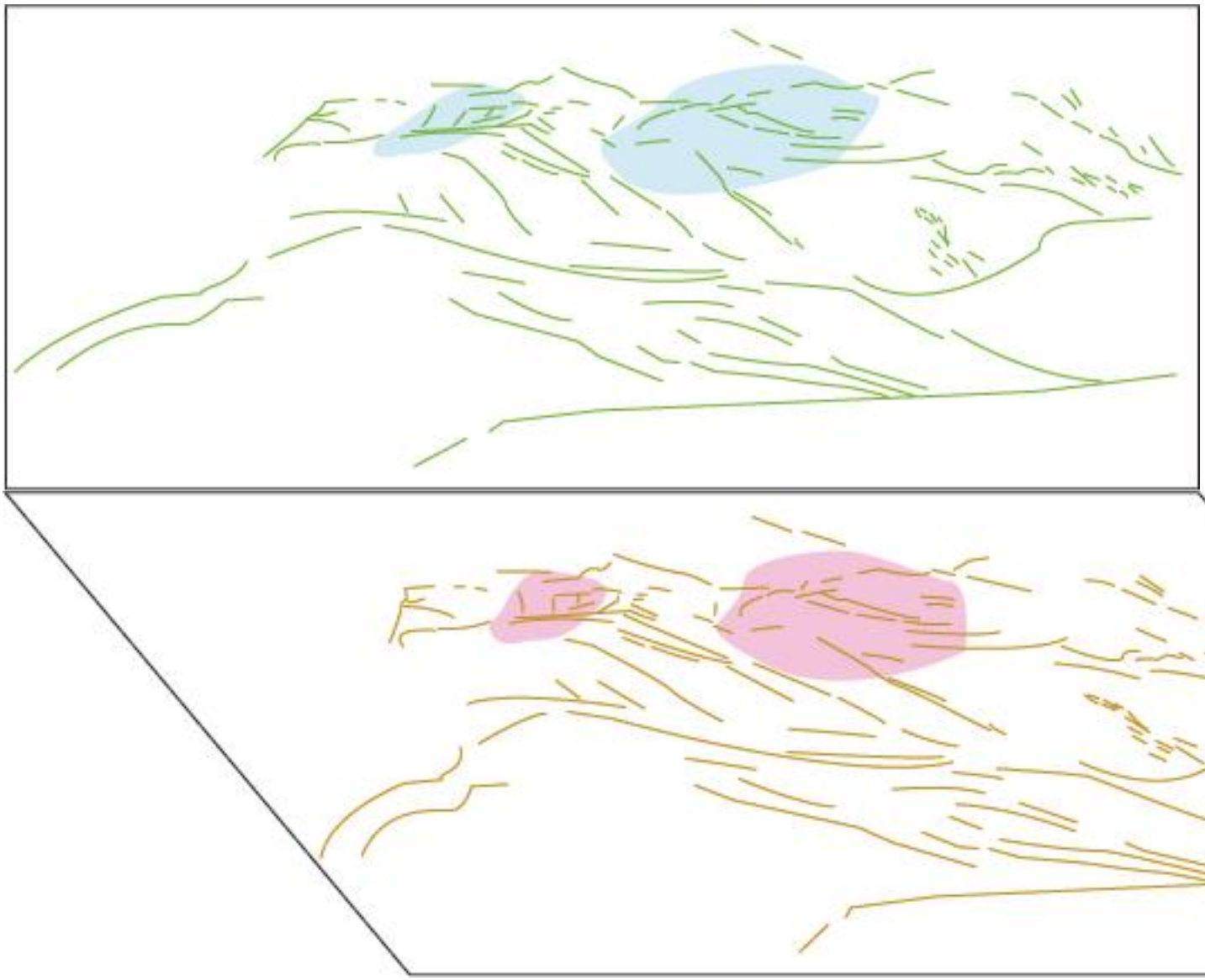

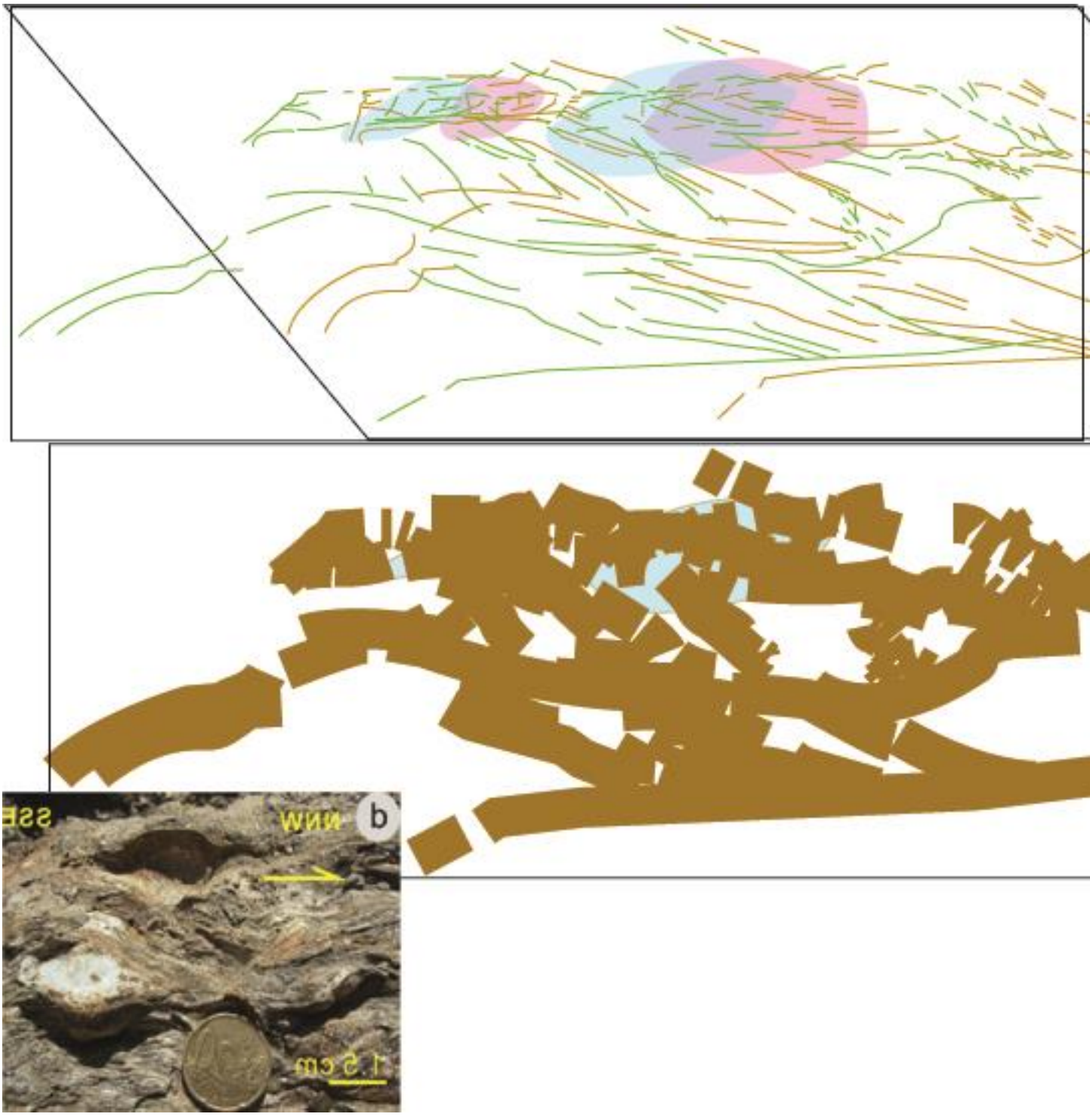
b
NNW
SSE
1.5 cm